

Quasiparticle exciton representation of frequency dispersed optical nonlinearities of conjugated polyenes

Hong Xiang Wang and Shaul Mukamel

Department of Chemistry, University of Rochester, Rochester, New York 14627

(Received 27 March 1992; accepted 18 August 1992)

The frequency dispersion of $\chi^{(3)}$ of conjugated polyenes is calculated using equations of motion which provide an anharmonic (exciton) oscillator picture. Quantum confinement of the relative electron-hole motion is shown to play an important role in determining the magnitude of $\chi^{(3)}$. The nature of the two-photon resonance observed in two-photon absorption and third harmonic generation is discussed, and the electroabsorption spectrum is calculated for a broad range of polyene sizes with up to 160 double bonds.

I. INTRODUCTION

The frequency dispersion of nonlinear optical susceptibilities such as $\chi^{(3)}$ of conjugated polyenes provides a direct probe for the mechanism of the optical nonlinearities. This information is complementary to the off-resonant response, which is most relevant for optical material applications.¹⁻⁴ The optical response of conjugated molecules is usually calculated using a molecular picture which is based on the molecular (many-electron) eigenstates. The molecular methods are exact in principle and Coulomb interactions and electron correlations can be incorporated with arbitrary accuracy, limited only by computation time. They can be classified into two major types, depending on the way they treat the optical response. The first is based on time-dependent perturbation theory, which relates the optical response to the properties of the excited states. This approach involves calculations of excited state properties (energies and transition dipoles) followed by multiple summations over states. Both steps become very tedious for large molecules.⁵⁻¹⁶ The second type of methods are based on a variational and perturbative treatment of the ground state, in the presence of the external electric field. Examples are the coupled Hartree-Fock (CHF) theory,^{10,11,16} where the susceptibilities are evaluated by a numerical differentiation of the self-consistent-field (SCF) energy of molecules in the presence of an electric field, with respect to the field, and the coupled-perturbed Hartree-Fock (CPHF), also known as time-dependent Hartree-Fock (TDHF),^{12,13,15} which is an analytical differentiation method. The CPHF method can be combined with numerous other quantum statistical techniques. For example, when the zeroth-order Hamiltonian is chosen as the Fock operator in the Rayleigh-Schrödinger perturbation theory (RSPT), the electron correlation (the error in the Hartree-Fock approach) can be included by the Møller-Plesset (MP) perturbation theory. The Rayleigh-Schrödinger double perturbation theory (RSPT) [also known as many-body perturbation theory (MBPT)]¹⁴ starts with the Hartree-Fock (HF) zero-order Hamiltonian and treats both electron correlations and the external electric field as a perturbation. Coupled cluster (CC) calculations¹⁵ can include higher-order electron correlations effectively.

The various methods for calculating the electronic structure of conjugated molecules up to the 60's were summarized by Salem.¹⁷ More recent developments can be found in Refs. 1-4. Two types of basis sets [the molecular orbitals (MO) and the valence bond (VB) orbitals] are commonly used, differing by their treatment of electron correlations. MO overestimates ionic contributions which VB totally ignores. The molecular orbital basis set plus configuration interaction is equivalent to the valence bond orbital basis set plus ionic configurations.⁴ Virtually all theoretical modeling of conjugated polyenes focuses explicitly only on the π electrons, while the σ electrons are only considered in a mean field way. The commonly used free electron models which neglect electron correlation are the Hückel model, or the Su-Schrieffer-Heeger (SSH) model when the electron-phonon coupling is included.¹⁸ The Pariser-Parr-Pople (PPP) model is often used to include electron correlations.⁴ Schulten, Ohmine, and Karplus¹⁹ have calculated the electronic structure of small polyenes, using four different basis sets: (1) SCF-MO, which includes only single excited configurations; (2) SCF-MO which also includes the double excitation configurations; (3) restricted valence bond basis (RV), which includes only the orthogonal atomic orbital valence bond structure accounted for effectively by the Heisenberg spin Hamiltonian, namely, all covalent structures and all structures generated from them by moving a single electron to its adjacent site; and (4) complete basis (c), for which the choice of starting function is immaterial. Their numerical results for the energy levels using these four basis sets show that except for the first, all other basis sets are in good agreement with experiment.²⁰ Recently, Kohler demonstrated the importance of the double excitation configurations to the electron correlations.^{20(c)} As another example of the application of the valence bond basis set, Soos and Ramasesha,²¹ using the PPP Hamiltonian, have calculated the electronic properties and the linear and the nonlinear optical (NLO) response of linear conjugated molecules with up to six double bonds, and obtained very good agreement with experiment.²²

A completely different approach for calculating the optical response is based on a semiconductor (as opposed to a molecular) viewpoint.^{18,23-28} This approach focuses on calculating the elementary excitations (quasiparticles) of

the system using Green's function techniques rather than the complete set of eigenstates. Its advantages are the clear physical picture of the origin of the NLO processes and the inclusion of electron–electron and electron–hole interactions, exciton response, and phonon effects from the very beginning. Using a simple basis set or the effective mass approximation, it is possible to derive analytical expressions for the linear and NLO responses of the system. These calculations can be extended easily to large molecules. The present theory is based on the semiconductor approach.²⁸

Extensive experimental effort was devoted to measuring the linear and NLO response of conjugated polyenes, either in liquids, solids, or thin films. The experimental techniques employed include linear absorption, fluorescence, reflection, electroabsorption, electroreflection, second harmonic generation (SHG), third harmonic generation (THG), two-photon absorption (TPA), and pump-probe experiments.^{20,29–33} The linear absorption experiments yield the transition energy (i.e., the band gap) from the highest occupied molecular orbital (HOMO) to the lowest occupied molecular orbital (LUMO). The results show that the 2^1A_g state is below the 1^1B_u state. The dispersed THG spectrum for polyacetylene in the energy range of 0.38–1.1 eV was first measured by Etemad and co-workers using the free electron laser. That work shows two resonances below the band gap which were interpreted as three- and two-photon resonance. Additional nonlinear optical spectral measurements (including the measurements of the amplitude, the phase, and the different tensor elements of the second- and third-order nonlinear optical susceptibilities) were made for different materials.³¹ The THG and TPA spectra demonstrate that the single-photon or three-photon transition allowed states are different from the two-photon allowed state. The two-photon resonance shows up therefore not exactly at half of the band gap. Recently the optical response of polysilanes had been studied by Koda, Hochstrasser, Kepler, Miller, and their co-workers.³⁴ Polysilanes are characterized by delocalized σ electrons and their nonlinear optical responses closely resembles that of conjugated- π systems. Resonant and off-resonant ultrafast $\chi^{(3)}$ measurements such as pump-probe, transient grating, optical stark, and coherent Raman by Etemad, Thakur, Baker, and their co-workers, reveal useful information regarding the exciton dynamics in these systems.³³

The magnitude of the nonlinear response and its scaling with size also received considerable attention. Strong electron correlations in virtual two-photon states have been argued to be the origin of unusually large nonresonant third-order susceptibility.⁹ For centrosymmetric conjugated chains, the eigenstates have a definite parity of the 1A_g or 1B_u type, and the one-photon transition moment vanishes between states of like parity. Since the ground state is 1A_g , it is evident that the π -electronic states in a third-order process must be connected in the series $^1A_g \rightarrow ^1B_u \rightarrow ^1A_g \rightarrow ^1B_u \rightarrow ^1A_g$. Virtual transitions to both one-photon and two-photon states are necessarily involved. The pathway involving m^1A_g states other than the ground

1A_g state makes the major contribution to the NLO response. There are only few *essential* one-photon and two-photon states. The two-photon states found by Garito and co-workers⁹ contain about 60% of doubly excited configurations for small size polyenes. As the molecular size increases, significant contributions from the increasingly large number of both 1A_g and 1B_u states result in the large enhancement of NLO response. Power law scaling of $\chi^{(3)} \sim N^b$ has been observed⁹ over a limited range of molecular sizes $N \sim 2$ –10 double bonds, with an exponent b of about 4.6. Understanding the response of these 1A_g and 1B_u excited states and their effects on the magnitude and the response time scale of large polyenes constitutes an important experimental and theoretical challenge.

In this paper, we develop a systematic method for calculating the linear and NLO responses of conjugated linear polyenes by adopting the semiconductor (rather than the molecular) approach. Starting with the PPP model and using the Heisenberg equations of motion for nonlocal two-particle (electron–hole) dynamical variables, we rigorously establish an anharmonic-oscillator picture for the nonlinear optical response. Analytical expressions are obtained for the optical susceptibilities, which provide a clear picture for the effects of different transitions as well as Coulomb and exchange interactions.

Anharmonic-oscillator modeling of optical nonlinearities have been suggested as a qualitative model since the early days of nonlinear optics³⁵ and the picture has been derived microscopically recently for Frenkel excitons in molecular aggregates with localized electronic states.²³ In an earlier study, we have analyzed the linear optical response of conjugated polyenes using this approach.²⁸ In addition, we have established the charge-transfer exciton nature of the elementary optical excitations of conjugated polyenes which are intermediate between the molecular (Frenkel) and the semiconductor (Wannier) excitons.³⁶ The scaling of the nonlinear response with size can therefore be directly related to other recent studies of molecular and semiconductor nanostructures.²⁵ The issue of the universality (material-independent) nature of the response raised recently³⁷ can therefore be addressed.

The remainder of this paper is divided as follows: In Sec. II, we present the two-band PPP Hamiltonian. In Sec. III, we derive the equation of motion in the Wannier representation. In Sec. IV, we calculate $\chi^{(3)}$ for the PPP model. In Sec. V, we present numerical calculations which show the dynamics of excitons and establish a correlation between size scaling of $\chi^{(3)}$ and quantum confinement of excitons. We further show the frequency dispersion of resonant third harmonic generation (THG), two-photon absorption (TPA) and electroabsorption, and discuss the origin of the two-photon resonance observed in these measurements.

II. ELECTRON–HOLE REPRESENTATION OF THE PPP HAMILTONIAN

The present theory starts with the Pariser–Parr–Pople (PPP) Hamiltonian which consists of the tight-binding single-electron (Hückel) Hamiltonian with the addition of

Coulomb interactions.^{4,28} In this section, we introduce the PPP Hamiltonian and recast it using an electron-hole representation which will be used throughout this paper. We start with the Hückel model Hamiltonian,

$$H_0 = \sum_{n=1}^N |2n\rangle \bar{\beta}(1-\delta) \langle 2n+1| + |2n\rangle \bar{\beta}(1+\delta) \langle 2n-1|, \quad (1)$$

where $|n\rangle$ represents an electron in the $2p_z$ orbital at the n th carbon atom. This Hamiltonian depends on two parameters $\bar{\beta}(1+\delta)$ and $\bar{\beta}(1-\delta)$ which represent the alternate couplings of the π electrons along the molecular chain. The eigenvalue problem $H_0\Phi = E\Phi$ of the Hückel model for a polyene with N double bonds can be exactly solved. The N lower (higher) eigenstates Φ_{vk} (Φ_{ck}) constitute the valence (conduction) band with energies ϵ_{vk} (ϵ_{ck}), respectively. Using periodic boundary conditions

$$\Phi_{vk}(N+1) = \Phi_{vk}(1), \quad (2)$$

the eigenvalues and eigenstates are given by^{5,17}

$$\Phi_{vk}(x) = \frac{1}{\sqrt{2N}} \sum_{m=1}^N e^{ikm} [f_2^m(x) e^{if(k)} \pm f_1^m(x)], \quad (3)$$

$$\epsilon_{vk} = \pm \bar{\beta} \sqrt{2} [(1+\delta^2) + (1-\delta^2) \cos k]^{1/2}, \quad (4)$$

$$\tan \left[\frac{f(k)}{2} \right] = \frac{(1-\delta) \sin(k)}{(1+\delta) + (1-\delta) \cos(k)}, \quad (5)$$

$$k = 2\pi j/N, \quad (6)$$

where $j=1,2,\dots,N$. The + and - signs in Eqs. (3) and (4) stand for $v=c$ (conduction band) and $v=v$ (valence band), respectively. $f_1^m(x) = \langle x|2m-1\rangle$ and $f_2^m(x) = \langle x|2m\rangle$ are the atomic $2p_z$ functions creating the m th double bond. Using these band functions, we construct a new basis set of *Wannier functions*

$$W_{v,n}(x) = \frac{1}{\sqrt{N}} \sum_k e^{ikn} \Phi_{vk}(x). \quad (7)$$

It can be verified easily that the Wannier functions at different sites are real and form an orthonormal basis of localized electronic states $\langle W_{v,n}|W_{v',m}\rangle = \delta_{v,v'} \delta_{nm}$, where $W_{v,n}$ is localized on the n th double bond. We next introduce creation and annihilation operators corresponding to the Wannier basis. c_n^\dagger creates an electron in the $W_{c,n}(x)$ state and d_n^\dagger creates a hole in (removes an electron from) the $W_{v,n}(x)$ state. The corresponding annihilation operators are c_n and d_n . These operators satisfy the Fermi commutation rules

$$[c_n, c_m^\dagger] = \delta_{nm} - 2c_n^\dagger c_n, \quad (8a)$$

$$[d_n, d_m^\dagger] = \delta_{nm} - 2d_n^\dagger d_n. \quad (8b)$$

All other commutators $[c_n, d_m^\dagger]$ etc. not given in Eq. (8) vanish. The polyenes are thus modeled as one-dimensional semiconductors. $c_n^\dagger c_n$ and $d_n^\dagger d_n$ create or annihilate an electron or a hole at the n th unit cell. The Hückel Hamiltonian in the Wannier basis then reads (for a detailed derivation see Appendix A)

$$H_0 = \sum_{nm} (c_n^\dagger c_m H_{nm}^c - d_m^\dagger d_n H_{nm}^v). \quad (9)$$

H_{nm}^v with $v=c,v$ are the matrix elements of the Hückel Hamiltonian in the Wannier basis

$$\langle W_{v,n}|H_0|W_{v',m}\rangle \equiv H_{nm}^v \delta_{vv'}. \quad (10)$$

Using Eq. (7), we get

$$H_{nm}^v = \pm \frac{\bar{\beta} \sqrt{2}}{N} \sum_k e^{-ik(n-m)} \epsilon_{vk}. \quad (11)$$

The + and - signs in Eqs. (11) and (10) stand for $v=c$ (conduction band) and $v=v$ (valence band), respectively. The Coulomb interaction between two electrons located at x and x' is modeled using the Ohno formula⁴

$$Z(x-x') = U \{1 + [(x-x')/q^2 U]^2\}^{-1/2}, \quad (12)$$

q being the electron charge and U is the on-site Hubbard interaction energy.

The total PPP Hamiltonian (H) for a polyene, constructed by adding the Coulomb interactions between the π electrons to the Hückel Hamiltonian, is finally given by

$$H = H_0 + H' + H_{\text{int}}, \quad (13)$$

where the Coulomb interaction part H' reads (see Appendix A)

$$H' = \sum_{nm} \left[\frac{1}{2} V_1(nm) (c_n^\dagger c_m^\dagger c_m c_n + d_m^\dagger d_n^\dagger d_n d_m - 2c_n^\dagger c_n d_m^\dagger d_m) + V_2(nm) c_n^\dagger c_n d_m^\dagger d_n \right]. \quad (14)$$

$V_1(nm)$ is the Coulomb and $V_2(nm)$ is the exchange interaction between two charges in two Wannier states localized at the n th and m th double bonds. These interactions may be expressed in terms of the matrix element

$$V \left(\begin{matrix} n_1 n_2 n_3 n_4 \\ v_1 v_2 v_3 v_4 \end{matrix} \right) \equiv \int \int W_{v_1, n_1}^*(x) W_{v_2, n_2}^*(x') Z(x-x') \times W_{v_3, n_3}^*(x') W_{v_4, n_4}^*(x) dx' dx, \quad (15)$$

where $v_j=c, v$ is the band index, and n_j denotes the position of the Wannier function along the chain. When the overlap of the Wannier functions is neglected, Eq. (15) vanishes unless $n_1=n_2$ and $n_3=n_4$, and we get

$$V_1(nm) = V \left(\begin{matrix} nmmn \\ vvvv \end{matrix} \right) = V \left(\begin{matrix} nmmn \\ cvvc \end{matrix} \right) = V \left(\begin{matrix} nmmn \\ vccv \end{matrix} \right) = V \left(\begin{matrix} nmmn \\ cccc \end{matrix} \right), \quad (16)$$

$$V_2(nm) = V \left(\begin{matrix} nmmn \\ cvcv \end{matrix} \right) = V \left(\begin{matrix} nmmn \\ vccv \end{matrix} \right). \quad (17)$$

As a result of the exchange interaction $V_2(nm)$, the excited states may become delocalized even in molecular crystals where the electrons are localized. This interaction is also responsible for the Förster mechanism of energy

transfer among organic molecules in condensed phases. The Coulomb interaction $V_1(nm)$ on the other hand affects the relative motion of the electron-hole pair and may create bound (exciton) states.

H_{int} denotes the interaction Hamiltonian between the molecule and the external electric field $E(\mathbf{r}, t)$,

$$H_{\text{int}} = - \sum_{nm} P_{nm} \cdot E[(n+m/2), t], \quad (18)$$

where $E[(n+m/2), t]$ is the electric field at the position $(n+m)/2$. P_{nm} denotes the contribution of a coherence between the n and m bonds to the optical polarization and is given by (see Appendix A)

$$P_{nm} = \mu_{nm}^c c_n^\dagger c_m - \mu_{nm}^v d_n^\dagger d_m + \mu_{nm}^{vc} c_n^\dagger d_m^\dagger + \mu_{nm}^{cv} d_m c_n. \quad (19)$$

μ_{nm}^{cv} is the interband transition dipole

$$\mu_{nm}^{cv} \equiv q \int W_{c,n}^*(x) x W_{v,m}(x) dx, \quad (20)$$

and μ_{nm}^c and μ_{nm}^v are the intraband transition dipoles

$$\mu_{nm}^c = \mu_{nm}^v \equiv q \int W_{c,n}^*(x) x W_{c,m}(x) dx. \quad (21)$$

Since the Hamiltonian does not depend on spin, the electron and the hole created by the dipolar interaction with the external fields must carry an opposite spin (i.e.,

they form a singlet exciton). For clarity, we have therefore omitted the spin label in the present notation. Using translational symmetry, it follows that $V_1(nm)$, $V_2(nm)$, μ_{nm}^c and μ_{nm}^{cv} depend only on the relative separation $n-m$ of the two bonds. Explicit expressions for these quantities will be given in Sec. IV following a change in notation to account for translational symmetry.

III. EQUATIONS OF MOTION IN REAL SPACE

Equation (19) expresses the polarization operator in terms of nonlocal (two-site) creation and annihilation operators. We shall introduce the following notation for these binary variables:

$$Y_{nm}^\dagger \equiv c_n^\dagger d_m^\dagger, \quad Y_{nm} \equiv d_n c_m, \quad C_{nm} \equiv c_n^\dagger c_m, \quad D_{nm} \equiv d_n^\dagger d_m. \quad (22)$$

The commutation relations of these operators are given in Appendix B. Using these definitions, the polarization operator (19) assumes the form

$$P_{nm} = \mu_{nm}^{vc} Y_{nm} + \mu_{nm}^{cv} Y_{nm}^\dagger + \mu_{nm}^c C_{nm} - \mu_{nm}^v D_{nm}. \quad (23)$$

The Heisenberg equation $\dot{A} = i/\hbar(H, A)$, together with the Hamiltonian (13) and the commutation relations (8a)–(8b) and (B1) to (B7), results in the following equations of motions for Y_{nm} , C_{nm} , and D_{nm}

$$\begin{aligned} -i\hbar\dot{Y}_{nm} = & - \sum_{m'} [\omega_{mm'}^c Y_{nm'} + \omega_{m'n}^v Y_{m'm} - E(t) (\mu_{mm'}^{cv} \delta_{nm'} - \mu_{m'n}^{cv} C_{m'm} - \mu_{mm'}^{vc} D_{m'n} + Y_{nm'} \mu_{mm'}^c - Y_{m'm} \mu_{m'n}^v)] + i\Gamma Y_{nm} \\ & - \sum_{m'} \{ [V_1(mm') - V_1(nm')] C_{m'm'} Y_{nm} + [V_1(nm') - V_1(mm')] D_{m'm'} Y_{nm} + V_2(nm') C_{m'n} Y_{m'm} \\ & + V_2(mm') D_{m'm} Y_{nm'} \} - V_2(nm) Y_{mn} + V_1(nm) Y_{nm} \end{aligned} \quad (24a)$$

$$\begin{aligned} -i\hbar\dot{C}_{nm} = & \sum_{m'} [(\omega_{m'n}^c C_{m'm} - \omega_{mm'}^c C_{nm'}) + E(t) (\mu_{mm'}^{cv} Y_{m'n}^\dagger - \mu_{m'n}^{vc} Y_{m'm} - C_{m'm} \mu_{m'n}^c + C_{nm'} \mu_{mm'}^c)] \\ & + \sum_{m'} [-C_{nm} V_1(nm) \delta_{m'n} + C_{m'm'} V_1(nm') \delta_{mn} + C_{nm} V_1(0) \delta_{m'n} - C_{nm} V_1(mm')] + i\Gamma C_{nm}, \end{aligned} \quad (24b)$$

$$\begin{aligned} -i\hbar\dot{D}_{nm} = & - \sum_{m'} [(\omega_{m'n}^v D_{m'm} - \omega_{mm'}^v D_{nm'}) + E(t) (\mu_{m'm}^{cv} Y_{nm'}^\dagger - \mu_{nm'}^{vc} Y_{mm'} + D_{m'm} \mu_{m'n}^v - D_{nm'} \mu_{mm'}^v)] \\ & + \sum_{m'} [-D_{nm} V_1(nm) \delta_{m'n} + D_{m'm'} V_1(nm') \delta_{mn} + D_{nm} V_1(0) \delta_{m'n} - D_{nm} V_1(mm')] + i\Gamma D_{nm}, \end{aligned} \quad (24c)$$

where ω_{nm}^c denotes the electron site energy (when $n=m$) and hopping matrix elements (when $n \neq m$). ω_{nm}^v are the corresponding quantities for the hole

$$\hbar\omega_{nm}^c = H_{nm}^c + \delta_{nm} \sum_{n'} [V_1(n'n) - V_2(nn)], \quad (25a)$$

$$\hbar\omega_{nm}^v = H_{nm}^v + \delta_{nm} \sum_{n'} [V_1(nn) - V_1(n'n)]. \quad (25b)$$

All operators in Eq. (24) are taken at time t . The equation for Y_{nm}^\dagger is simply the Hermitian conjugate of the equation for Y_{nm} . The calculation of resonant experiments requires the inclusion of relaxation processes. In Eqs. (24), we have therefore added a phenomenological relaxation rate Γ which is common for the electron, hole, and electron-hole pair variables. This parameter may represent a finite lifetime, dephasing, or a finite spectral resolution. Equations

tions (24) are not closed. They contain in the right-hand side new higher-order dynamical variables, namely, $C_{n'm'}Y_{nm}$ and $D_{n'm'}Y_{nm}$. A rigorous way to proceed is to use the Heisenberg equation to derive more equations for these new variables. This procedure will eventually generate an infinite hierarchy of equations. In this paper, we close the hierarchy by taking expectation values of Eq. (24) and then making the factorizations

$$\langle C_{n'm'}Y_{nm} \rangle = \langle C_{n'm'} \rangle \langle Y_{nm} \rangle, \quad (26a)$$

$$\langle D_{n'm'}Y_{nm} \rangle = \langle D_{n'm'} \rangle \langle Y_{nm} \rangle. \quad (26b)$$

Equations (26) go beyond the standard random phase approximation (RPA)³⁸ since by adopting this factorization, we still retain the coupling between different electron-hole pairs.

Equations (24) together with the factorizations [Eqs. (26)] form the basis for the theory developed in this article. They map the calculation onto the dynamics of N^2 , $N(N-1)/2$, and $N(N-1)/2$ relevant oscillators representing electron-hole pairs ($\langle Y_{nm} \rangle$), electron coherence ($\langle C_{nm} \rangle$), and hole coherence ($\langle D_{nm} \rangle$), respectively, for a total number of $N(2N-1)$ oscillators. Note that $\langle Y_{nm} \rangle$, $\langle C_{nm} \rangle$, and $\langle D_{nm} \rangle$ constitute a minimal set of relevant variables since the polarization depends explicitly on all of them. In the Hückel model where we set $V_1 = V_2 = 0$, the new operators (26) never appear, so that our procedure is exact and the hierarchy is closed using our $N(2N-1)$ oscillators. The linear and the NLO responses will be calculated in the up coming sections by solving these equations perturbatively in the radiation field.

IV. $\chi^{(3)}$ FOR THE PPP MODEL

In the ground (vacuum) state of the Hückel model, all of the N valence-band states are occupied by two electrons. Upon optical excitation, an electron may move from the ground state to any of the unoccupied states in the conduction band, creating a hole in the valence band. The lowest transition energy is from the top of the valence band (HOMO) to the bottom of the conduction band (LUMO). This picture changes once the electron-hole Coulomb interactions are incorporated in the PPP Hamiltonian. The electron at site n and the hole at site m may form a bound exciton due to their attractive Coulomb interaction. The excitons are created coherently, but their interactions may destroy the coherence. Their coherence size is expected to control the optical response of the system.²³

Hereafter we assume a homogeneous excitation (the field does not depend on position). This is justified when the field is polarized along the chain, or, alternatively, when the polyene size is much smaller than the optical wavelength. The applied electric field in a third-order frequency-domain measurement is then given by

$$E(t) = \sum_{j=1}^3 (E_j e^{-i\omega_j t} + c.c.), \quad (27)$$

and the material-field interaction reads

$$H_{\text{int}} = -P \cdot E(t), \quad (28)$$

where the total polarization is

$$P \equiv \sum_{nm} P_{nm}. \quad (29)$$

The excitons undergo two types of motion—related to their translational motion along the molecular chain and the relative motion of the pair. The separate treatment of these two types of motion is best accomplished by transforming the binary variable coordinates as follows:

$$Y_{s,k} \equiv \frac{1}{\sqrt{N}} \sum_{r=1}^N e^{-ikr} d_{r+s/2} c_{r-s/2}, \quad (30a)$$

$$Y_{s,k}^\dagger \equiv \frac{1}{\sqrt{N}} \sum_{r=1}^N e^{ikr} c_{r-s/2}^\dagger d_{r+s/2}^\dagger, \quad (30b)$$

$$C_{s,k} \equiv \frac{1}{\sqrt{N}} \sum_{r=1}^N e^{-ikr} c_{r+s/2}^\dagger c_{r-s/2}, \quad (30c)$$

$$D_{s,k} \equiv \frac{1}{\sqrt{N}} \sum_{r=1}^N e^{ikr} d_{r-s/2}^\dagger d_{r+s/2}. \quad (30d)$$

Here r is the translational coordinate and s is the relative motion. To exploit the translational symmetry of the problem, we treat the translational motion in momentum (k) space. Using these transformed variables, the polarization operator is given by

$$P = \sum_{s,k} [\mu_s (Y_{s,k} + Y_{s,k}^\dagger) + \mu_{s,k}^c (C_{s,k} + D_{s,k})], \quad (31)$$

where we have defined

$$\mu_s \equiv \frac{1}{\sqrt{N}} \sum_r e^{-ikr} \mu_{r+s/2, r-s/2}^{cv}, \quad (32a)$$

$$\mu_{s,k}^c = \mu_{s,k}^v \equiv \frac{1}{\sqrt{N}} \sum_r e^{-ikr} \mu_{r+s/2, r-s/2}^c \equiv \mu'_s \delta_{k,0} + g_k \delta_{s,0}. \quad (32b)$$

Explicit expressions for these matrix elements are

$$\mu_s = \frac{1}{2N^2} \sum_{k,k',n'=1}^N \exp[-i(k-k')n' + i(k+k')s/2] \times (\exp\{i[f(k) - f(k')]\} - 1)(n' - s) + \frac{1}{2} \delta_{s,0}, \quad (33a)$$

$$\mu'_s = \frac{1}{2N^2} \sum_{k,k',n'=1}^N \exp[-i(k-k')n' + i(k+k')s/2] \times (\exp\{i[f(k) - f(k')]\} + 1)(n' - s), \quad (33b)$$

$$g_k = \frac{1}{\sqrt{N}} \sum_{r=1}^N r e^{-ikr}. \quad (33c)$$

Setting $s = n - m$, we obtain for the Coulomb and exchange interactions

$$\begin{aligned}
 V_j(s) = & 1/4V(s) + (-1)^j/(4N^2) \sum_{k,k',n'} \left\{ Z(s/2+n'+1/2)\exp\{-i[f(k)-f(k')+(n'+s/2)(k-k')]\} \right. \\
 & \left. + Z(s/2-n'+1/2)\exp\{-i[f(k)-f(k')+(n'-s/2)(k-k')]\} \right\} + 1/(4N^2) \sum_{n_1,n',k_1,k_2,k'} Z(n_1-n') \\
 & \times \exp\{-i[f(k')-f(k_1)+f(k)-f(k_2)+(n'-s/2)(k-k_2)+(n_1+s/s)(k'-k_1)]\}, \tag{34}
 \end{aligned}$$

where $j=1,2$. $Z(s)$ is Ohno's formula (12) for the Coulomb interaction. We further introduce two auxiliary quantities

$$\omega_s^c = \pm \bar{\beta}/\sqrt{2} \sum_k e^{-iks} \epsilon_{ck} + \delta_{s,0} \sum_{s'} [V_1(s') - V_2(0)], \tag{35}$$

$$\omega_s^v = \pm \bar{\beta}/\sqrt{2} \sum_k e^{-iks} \epsilon_{vk} + \delta_{s,0} \sum_{s'} [V_1(0) - V_1(s')], \tag{36}$$

where $\epsilon_{\nu k}$ are given by Eq. (4) with $\nu=c,v$. The variation of μ, ω, V_1 , and V_2 with s was calculated earlier.²⁸

In Appendix C, we present the equations of motion for the PPP model [Eq. (24)] using the transformed variables [Eqs. (30)]. We have solved these equations of motion by expanding the expectation values of all operators in powers of the external field, and solving for $\langle Y_{s,k} \rangle, \langle C_{s,k} \rangle, \langle D_{s,k} \rangle$, and the polarization order by order. The following calculations were performed in the frequency domain, where the optical polarization is given by

$$\begin{aligned}
 \langle P(\omega) \rangle = & \sum_{s,k} \{ \mu_s [\langle Y_{s,k}(\omega) \rangle + \langle Y_{s,k}^\dagger(\omega) \rangle] \\
 & + \mu_{s,k}^c [\langle C_{s,k}(\omega) \rangle + \langle D_{s,k}(\omega) \rangle] \}. \tag{37}
 \end{aligned}$$

We have adopted the definition of a Fourier transform

$$A(\omega) = \frac{1}{\sqrt{2\pi}} \int_{-\infty}^{\infty} dt e^{-i\omega t} A(t), \tag{38}$$

where $A = Y_{s,k}, C_{s,k}$, and $D_{s,k}$.

The solution of the equations of motion and the optical response may be expressed most conveniently in terms of Green's functions representing the electron and the hole motions. These Green's functions are introduced below through the solution of our equations of motion to first and second order in the radiation field. We thus have

$$\langle Y_{s,k}^{(1)}(\omega) \rangle = \sum_{s'} G_{s,s'}(k,\omega) \mu_{s'} \bar{E}(\omega) \delta_k, \tag{39a}$$

$$\begin{aligned}
 \langle Y_{s,k}^{(2)}(\omega) \rangle = & \sum_{s',s_1,s_2} 2G_{s,s'}(k,\omega) [\mu'_{s_2-s'} \delta_{k,k'} + g'_{k-k'} \delta_{s_2,s'} \\
 & \times \sin(k's - ks')/2] G_{s_1,s_2}(k,\omega) \mu_{s_2} \\
 & \times E(\omega) E(\omega - \omega_1) \delta_{k,0}, \tag{39b}
 \end{aligned}$$

$$\langle C_{s,k}^{(2)}(\omega) \rangle = \sum_{s',s_1,s_2} F_{s,s'}(k,\omega) \{ \mu_{s_1+s'} \exp[ik(s'+s_1)/2]$$

$$\begin{aligned}
 & \times G_{s_1,s_2}(k, -\omega + \omega_1) - \mu_{s_1-s'} \\
 & \times \exp[ik(s'-s_1)/2] G_{s_1,s_2}(\omega - \omega_1) \} \\
 & \times \mu_{s_2} E(\omega) E(\omega - \omega_1) \delta_{k,0}, \tag{39c}
 \end{aligned}$$

$$\begin{aligned}
 \langle D_{s,k}^{(2)}(\omega) \rangle = & \sum_{s',s_1,s_2} Q_{s,s'}(k,\omega) [\mu_{s_1-s'} \exp[ik(s'-s_1)/2] \\
 & \times G_{s_1,s_2}(k, -\omega + \omega_1) - \mu_{s_1+s'} \\
 & \times \exp[-ik(s'+s_1)/2] G_{s_1,s_2}(\omega - \omega_1)] \\
 & \times \mu_{s_2} E(\omega) E(\omega - \omega_1) \delta_{k,0}. \tag{39d}
 \end{aligned}$$

Here the superscript denotes the order with respect to the applied field. The Green's function $G_{s,s'}(k,\omega)$ describes the motion of a single electron-hole pair and is given by

$$\begin{aligned}
 G_{s,s'}^{-1}(k,\omega) \equiv & \omega_{s'-s}^c \exp[-ik(s'-s)/2] \\
 & - \omega_{s'-s}^v \exp[ik(s'-s)/2] \\
 & + V_2(s) \delta_{s'-s} - [V_1(s) + \omega + i\Gamma] \delta_{s',s}, \tag{40}
 \end{aligned}$$

The motion of a single electron in the conduction band is described by the $F_{s,s'}(k,\omega)$ Green's function,

$$\begin{aligned}
 F_{s,s'}^{-1}(k,\omega) \equiv & 2\omega_{s'-s}^c \sin[k(s'-s)/2] - [V_1(s) - V_1(0) + \omega \\
 & + i\Gamma] \delta_{s',s} + \sum_{s''} [V_1(s'') \delta_{s',0} - V_1(s'') \delta_{s',s}]. \tag{41}
 \end{aligned}$$

Finally, the motion of a single hole in the valence band is given by the $Q_{s,s'}(k,\omega)$ Green's function

$$\begin{aligned}
 Q_{s,s'}^{-1}(k,\omega) \equiv & 2\omega_{s'-s}^v \sin[k(s'-s)/2] - [V_1(s) - V_1(0) + \omega \\
 & + i\Gamma] \delta_{s',s} + \sum_{s''} [V_1(s'') \delta_{s',0} - V_1(s'') \delta_{s',s}]. \tag{42}
 \end{aligned}$$

In the subsequent manipulations, we shall also use these Green's functions at $k=0$. We therefore further introduce the abbreviated notation

$$G_{s,s'}(\omega) \equiv G_{s,s'}(k=0,\omega), \tag{43}$$

$$F_{s,s'}(\omega) \equiv F_{s,s'}(k=0,\omega) = Q_{s,s'}(k=0,\omega). \tag{44}$$

The physical significance of these Green's functions is as follows: $G_{s,s'}(k,\omega)$ describes the translational and the relative motions of an electron hole pair. By taking $k=0$, we

assume a homogeneous (uniform) distribution of the pair, and the translational coordinate drops out of the problem; $G_{s,s'}(\omega)$ thus represents only the relative motion. Similarly $F_{s,s'}(\omega)$ describes the momentum dynamics of a homogeneously prepared electron (using the Wigner representation,^{23(c)} the electron momentum is the conjugate variable to s).^{26,27} $Q_{s,s'}(\omega)$ describes the momentum dynamics of a homogeneously prepared hole. Using these Green's functions, we can derive closed form expressions for the optical susceptibilities. For the linear response, we get

$$\chi^{(1)}(\omega) = \rho[\alpha(\omega) + \alpha(-\omega)] \quad (45)$$

with

$$\alpha(\omega) = \sum_{s,s'} \mu_s \mu_{s'} G_{s,s'}(\omega), \quad (46)$$

and ρ denotes the molecular number density. We next consider the third-order susceptibility. For a general four wave mixing process with three incoming fields ω_1, ω_2 , and ω_3 , generating a polarization at $\omega_f \equiv \omega_1 + \omega_2 + \omega_3$, we have

$$\begin{aligned} \chi^{(3)}(-\omega_f, \omega_1, \omega_2, \omega_3) \\ = \rho \sum_p [\gamma(\omega_1, \omega_2, \omega_3) + \gamma(-\omega_1, -\omega_2, -\omega_3)], \end{aligned} \quad (47)$$

with

$$\begin{aligned} \gamma(\omega_1, \omega_2, \omega_3) = & 2 \sum_{ss's_1s_2s_3s_4} \mu_s \mu_{s_4} \mu_{s_1+s'} \mu_{s_3-s_2} G_{s,s'}(\omega_f) F_{s_1,s_2}(\omega_1 + \omega_2) G_{s_3,s_4}(\omega_1) + \frac{4}{\sqrt{N}} \sum_{ss's_1s_2s_3kk'} \sin[k(s_3 - s'/2)] \\ & \times \sin(k's_1/2) \mu_s \mu_{s_2} \mu_{s_3-s'}^c \mu_{s_2,k}^c G_{s,s'}(k, \omega_f) G_{s_3,s_1}(k', \omega_1 + \omega_2) G_{s_1,s_2}(\omega_1) - \frac{2}{\sqrt{N}} \\ & \times \sum_{s's_1s_2s_3k} \sin(ks_1/2) \mu_{s_3+s'} \mu_{s_2} \mu_{s,k}^c \mu_{s_2,k}^c [F_{0,-s'}(k, \omega_f) - Q_{0,s'}(k, \omega_f)] [G_{s_3,s_1}(k, \omega_1 + \omega_2) \\ & + F_{s_1,s'}(\omega_1 + \omega_2)] G_{s_1,s_2}(\omega_1) + \sum_{ss's_1s_2s_3s_4s_5} V_2(s' - s_2) \mu_s \mu_{s_4} \mu_{s_1+s_4} \mu_{s_3} G_{s,s'}(\omega_f) [F_{s_2-s',s_1}(\omega_1 + \omega_2) \\ & + F_{s_2-s',-s_1}(\omega_1 + \omega_2)] G_{s_2,s_3}(\omega_1) G_{s_4,s_5}(\omega_2). \end{aligned} \quad (48)$$

The s summations run from 0 to $N-1$, the k summations run from 1 to N , and the p summation runs over all $3! = 6$ permutations of the three incoming frequencies ω_1, ω_2 , and ω_3 . All the terms in Eq. (48) contain three Green's function factors which, from right to left, describe the evolution of the system following the first, the second, and the third interactions with the external electric field.³⁹ In all the terms, the system's evolution is described by the electron-hole Green's function $G_{s,s_1}(\omega)$ between the first and the second interactions. The first term in Eq. (48) represents the contributions of interband transitions alone, with the electron or hole Green's functions $F_{s,s_1}(\omega)$ or $Q_{s,s_1}(\omega)$ describing the time evolution following the second interaction with the field. The second and third terms represent the combination of interband and intraband transitions. They contain two interband transition dipoles μ_s and two intraband transition dipoles $\mu_{s,k}^c$. In the second term, the

system's evolution is described solely by the electron-hole Green's functions $G_{s,s_1}(k, \omega)$ and $G_{s,s_1}(\omega)$. In the third term, the system's evolution is described by the electron or the hole Green's functions after the second interaction. The last term, which is proportional to the intermolecular Coulomb interaction, represents the local field correction. The numerical calculations of $\chi^{(3)}$ for a polyene with N double bonds involve the inversion of the $N \times N$ matrices $G_{s,s'}$, $F_{s,s'}$, and $Q_{s,s'}$ N times for each frequency.

In concluding this section, let us consider the nonlinear response of the Hückel model for which $V_1 = V_2 = 0$. Equation (48) then reduces to the form

$$\alpha^0 = \sum_{s,s'} \mu_s \mu_{s'} G_{s,s'}(\omega) \quad (49)$$

and

$$\begin{aligned} \gamma^0(\omega_1, \omega_2, \omega_3) = & \sum_p \left[\sum_{ss's_1s_2s_3s_4} 2\mu_s \mu_{s_4} \mu_{s_1+s'} \mu_{s_2-s_3} G_{s,s'}^0(\omega_f) F_{s_1,s_2}^0(\omega_1 + \omega_2) G_{s_3,s_4}^0(\omega_1) \right. \\ & \left. - 4/\sqrt{N} \sum_{ss's_1s_2s_3k} \sin(ks'/2) \mu_{s_1+s_2} \mu_{s_3} \mu_{s,k}^c \mu_{s_3-s',k}^c F_{s,s'}^0(k, \omega_f) F_{s_3,s_1}^0(k, \omega_1 + \omega_2) G_{s_2,s_3}^0(\omega_1) \right]. \end{aligned} \quad (50)$$

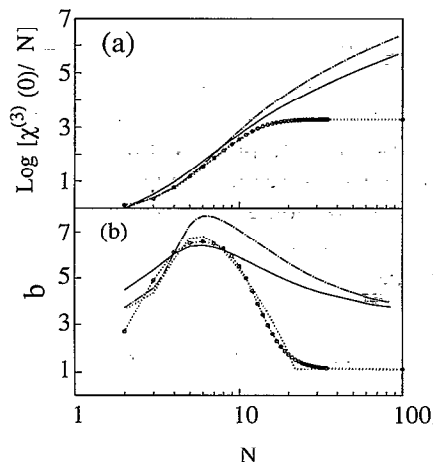


FIG. 1. (a) Variation of the static $\chi^{(3)}(0)$ per double bond with size N for polyacetylene $\delta=0.07$. (Solid line) Hückel model; (dashed-dotted line) Hückel model with cyclic boundary conditions [Eq. (2)]; (dotted line) PPP model; (circles) a fit with Eq. (51). (b) The scaling exponent $b \equiv d \log \chi^{(3)}/d \log N$ calculated using the slopes of the curves in (a).

Here the 0 superscript denotes that these quantities are calculated in the absence of Coulomb interactions. The Green's functions $G_{s,s'}^0$ and $F_{s,s'}^0$ are given by Eqs. (40) and (41) by setting the interactions $V_1=V_2=0$. Alternative expressions for α^0 and γ^0 for the Hückel model in terms of the single particle states (rather than the oscillator variables) is given in Appendix D. That expression which will be used as well in the following calculations does not depend on the periodic boundary conditions and allows the comparison of our results with more conventional theories.

V. CALCULATIONS AND DISCUSSION

A. Scaling and saturation of $\chi^{(3)}$ with size

In all calculations, we have used $\bar{\beta} = -2.4$ eV. δ was taken to be either 0.07 (polyacetylene) or 0.15 (polydiacetylene).⁴ In Fig. 1, we present the variation of the static $\chi^{(3)}(0)$ with N for polyacetylene. Shown is the PPP model with $U=11.26$ eV (dotted curve) as well as the Hückel model with cyclic boundary conditions (dashed-dotted). In addition, we show the exact solution to the Hückel model [Eq. (1)] obtained by numerical diagonalization of Eq. (9) without imposing any boundary conditions (solid curve). The scaling with size of $\chi^{(3)}(0)$ in the PPP model was fitted with the following Padé approximant (circles):

$$\chi^{(3)}(0)/N = [1 + (N/N_s')^5] / [1 + (N/N_s)^5], \quad (51)$$

where the saturation size is $N_s = 13.33$ and $N_s' = 2.94$. This fit is also displayed in Fig. 1. We note that for the PPP model, $\chi^{(3)}(0)/N$ shows a rapid nonlinear dependence on size for small sizes, which saturates for larger sizes where the thermodynamics limit is obtained. The saturation is seen clearly by considering the slope $b \equiv d \log \chi^{(3)}(0)/d \log N$ shown in the lower panel. The slope drops dramatically to $b=1$ at a critical size ($N=21$). It is interesting to note that the slope shown in Fig. 1(b) goes to 1 very abruptly in a nonanalytical fashion.³⁶ Equation (51) does

not reproduce this nonanalyticity and varies more smoothly across the critical value of N . The Hückel calculation behaves very differently. The exponent b reaches a maximum $b=6.2$ (numerical diagonalization) or 7.7 (cyclic boundary conditions) at $N=6$ and then approaches the value of $b=4$ for $N \approx 100$. The Hückel model thus does not saturate in the size range studied. Earlier approximate calculations using the Hückel model which include only a partial summation over states have predicted a saturation at the size of $N \approx 50$ [Ref. 40(a)] and $N \approx 40$ [Ref. 40(b)]. Our exact calculation is at variance with these results. Comparing the dashed-dotted and solid curves for the slope [Fig. 1(b)] shows how the effects of the boundary conditions decrease with polyene size, since boundary effects are less important for larger polyenes. The figure provides a justification for using the cyclic eigenstates, which offer a good qualitative picture for all sizes and lend themselves more easily to analytical calculations. In all the calculations presented hereafter, we have used the solution to the Hückel model with cyclic boundary conditions [Eq. (2)].

In order to explore the nature of the excitons in conjugated polyenes, we have calculated the time evolution of a single electron-hole pair following an impulsive (δ -function) excitation pulse at $t=0$. For simplicity, we further assumed that the polyene is small compared with the optical wavelength, so that the initial excitation is homogeneous ($k=0$). The initially prepared (unnormalized) doorway state is then

$$|\Phi(t=0)\rangle = P|0\rangle = \sum_s Y_{s,0}^\dagger |0\rangle, \quad (52)$$

P being the polarization operator (29). The probability of the pair to be separated by s lattice units at time t is then given by

$$P_s(t) = |A_s(t)|^2 / \sum_s |\mu_s|^2, \quad (53)$$

where

$$A_s(t) \equiv \sum_{s'=0}^{N-1} G_{s,s'}(k,t) \mu_{s'}, \quad (54)$$

where $G_{s,s'}(k,t)$ is the Fourier transform of $G_{s,s'}(k,\omega)$, i.e.,

$$G_{s,s'}(k,t) = \int e^{-i\omega t} G_{s,s'}(k,\omega) d\omega. \quad (55)$$

A useful measure of the degree of delocalization of the pair is the *inverse participation ratio*^{27,41}

$$\kappa(t) \equiv 1 / \sum_s P_s^2(t). \quad (56)$$

If the pair is distributed over M sites, then $P_s(t) \sim M^{-1}$ and therefore $\kappa \sim M$. In Fig. 2, we plot $\kappa(t)$ for different magnitudes of the Coulomb interaction U and sizes N . Panels 2(a) and 2(b) compare the behavior of $N=100$ with $U=0$ (Hückel) and $U=11.26$ eV (PPP) model. In both cases, the electron and the hole are created on the same bond so that initially $\kappa(0) \sim 1$ independent on the Coulomb interaction. The subsequent evolution is, however, very different. For the Hückel model [panel 2(a)], the

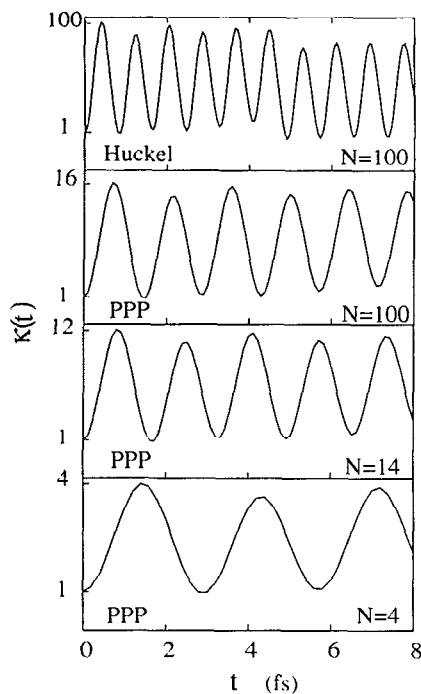


FIG. 2. The time-dependent inverse participation number $\kappa(t)$ for polyacetylenes ($\delta=0.07$) with different values of the Hubbard interaction U and size N . $U=0$ is the Hückel model; $U=11.26$ eV is the PPP model, as indicated.

pair is uncorrelated and the amplitude κ_m of the $\kappa(t)$ oscillation is equal to the polyene size 100. For the PPP model [panel 2(b)], the electron and the hole become tightly bound (localized) and κ_m decreases to 16. We interpret κ_m as the *exciton coherence size*. In the following panels 2(c) and 2(d), we vary the size N ($N=14$ and 4) for the PPP calculation. As long as the molecular size is larger than the coherence size, the amplitude is unaffected by N . $\kappa(t)$ for $N=30$ (not shown) is virtually identical to that of $N=100$. However, as the size decreases further, exciton confinement becomes significant and κ is affected strongly by N . The figure thus illustrates clearly the formation of a charge-transfer bound exciton with delocalization length κ_m which becomes more Frenkel-like as U is increased. The variation of the amplitude κ_m with size N and with U was shown to be remarkably similar to that of $\chi^{(3)}$ including the sharp nonanalytical behavior of the slope b' ($\kappa_m \sim N^{b'}$) at a critical size $N=18$.³⁶ We further expect the Hückel susceptibilities to saturate at much larger size due to a different (nonexcitonic) mechanism.³⁶

Another spectroscopic observable that is sensitive to exciton confinement is the band gap E_g which increases as N decreases, resembling the blue shifts in semiconductor nanostructure.²⁵ In Fig. 3, we display the variation of the band gap E_g , the amplitude of $\kappa(t)$ (κ_m), and $\log[\chi^{(3)}(0)/N]$ with molecular size N . For large N , all three quantities saturate at roughly the same size. The correlation between the exciton size and the saturation size of $\chi^{(3)}$ demonstrated in this figure was pointed out earlier.^{28,36}

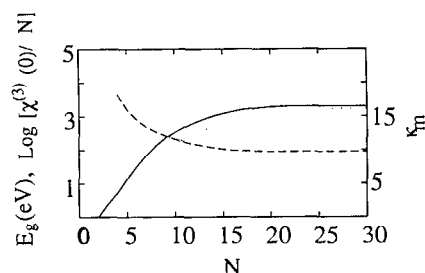


FIG. 3. The variation with molecular size of the band gap E_g (dashed-dotted line), the static nonlinear susceptibility $\log[\chi^{(3)}(0)/N]$ (solid line), and the participation ratio amplitude κ_m (dotted line) for polyacetylene ($\delta=0.07$).

B. Third harmonic generation

The amplitude of third harmonic generation (THG) signal per double bond is given by

$$S_{\text{THG}} = |\chi^{(3)}(-3\omega, \omega, \omega, \omega)/N|. \quad (57)$$

The signal is given by the square of S_{THG} . THG spectra of linear polyenes have been measured by many experimental groups^{22,31,32} and calculated using the sum over states expression.^{5,6,9,21} Two major resonances below the band gap were found in these studies. The lower frequency resonance is exactly at one-third of the band gap. The other resonance is close to, but not exactly at half of the band edge. It has been argued that the former is a three-photon resonance and the later is a two-photon resonance.⁴ Since the two-photon process and the three-photon process have different selection rules, they show different resonance energies. Using the PPP model and a diagrammatic valence-bond technique, Soos and co-workers were able to reproduce the experimental THG spectra of the $N=4$ polyene (octatetraene).²¹ However, the origin of this two-photon resonance and its variation with Coulomb interactions remains an open question, particularly for large molecules. In Fig. 4(a), we display the THG spectra of polyacetylene ($\delta=0.07$) for different molecular sizes ranging from four to 30 double bonds for both the Hückel and the PPP models. No two-photon resonance below the band gap E_g is found for the Hückel model with small molecular sizes ($N=4,10$). As the molecular size is increased to 20 and 30, we find that the two-photon resonance frequency shifts below the band gap and is still higher than the midgap. This implies that the two-photon active A_g states and the one-photon B_u states become closer as N is increased, but the A_g state still lies above the B_u state. On the other hand, our calculation for the PPP model shows that this two-photon resonance is below half the band gap, which implies that the order of the A_g and B_u states is reversed. In the present formulation, this resonance comes from the electron Green's function $F_{s_1, s_2}(\omega_1 + \omega_2)$ and the hole Green's function $Q_{s_1, s_2}(\omega_1 + \omega_2)$. We find that the two-photon resonance involves the combination of intraband and interband transitions. In all the calculations presented in Fig. 4(a), except for $N=4$, we find several two-photon resonances between the band gap and one-third of the band

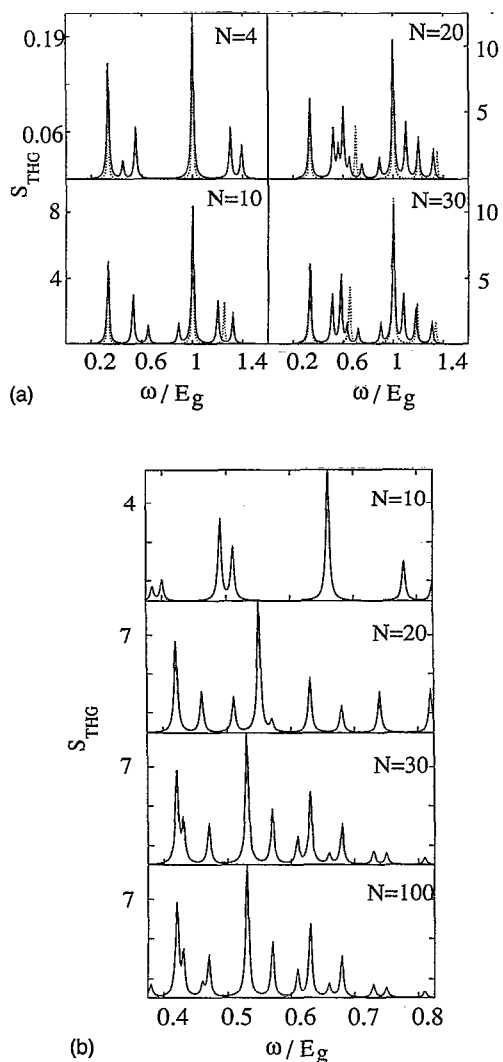


FIG. 4. (a) Third harmonic generation signal [Eq. (57)] for polyacetylenes ($\delta=0.07$) with different sizes. (Solid line) The PPP model with $U=11.26$ eV, (dotted line) the Hückel model. The x axis was scaled by the band gap which is different for both models. For $N=4, 10, 20$, and 30 , we found a band gap $E_g=3.62, 2.31, 1.88$, and 1.73 eV for the PPP model and $E_g=1.3, 1.1, 0.90$, and 0.87 eV for the Hückel model, respectively. The signal for the Hückel model was scaled with respect to the PPP model by a factor of 27, 15, 11, and 9 for $N=4, 10, 20$, and 30 , respectively. $\Gamma=0.08$ eV. (b) The two-photon region in (a) is shown with a higher resolution. $\Gamma=0.02$ eV.

gap, but the most intense line is always above half of the band gap in the PPP model. This demonstrates the *essential* states in the optical response of conjugated polyenes.^{7,9,20} The essential $2A_g$ state is below the essential $1B_u$ state. The two-photon resonance region is shown with a higher resolution in Fig. 4(b). The relative energy of the 1^1B_u and 2^1A_g states provides an important illustration for the effect of electron–electron interactions on the electronic structure. As shown by Kohler,²⁰ the energy of the 1^1B_u state in the Hückel model is lower than the energy of the 2^1A_g state, but in the PPP model, the order of these two electronic states may change.¹⁹ Therefore the relative position of the lowest frequency two-photon resonance in the THG spectrum with respect to the band gap should be a

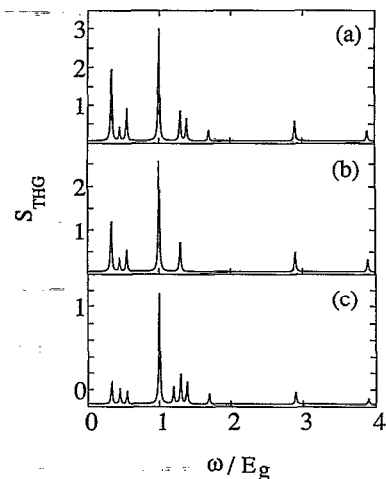


FIG. 5. Third harmonic generation signal [Eq. (57)] for polyacetylenes ($\delta=0.07$) for the PPP model with $N=4$, $U=11.26$ eV, and $\Gamma=0.08$ eV. (a) Total THG signal calculated from Eq. (48). (b) Contributions to the THG from transitions involving the interband transitions and the s -dependent part of the intraband transitions. (c) The contribution of the remaining terms [other than those shown in (b)].

clear signature of the effect of the Coulomb interactions on the relative position of the 2^1A_g and 1^1B_u states.

$\mu_{s,k}^c$ [Eq. 32(b)] has two contributions μ_s' and $g_k \cdot g_k$ is the k -dependence part of the intraband transition dipole, which describes intraband translational charge transfer. In order to explore the role of g_k in THG, we have plotted in Fig. 5(a) the total THG spectra, in Fig. 5(b) the separate contribution of g_k , and in Fig. 5(c) the remaining terms which do not depend on g_k . The terms proportional to g_k make more contributions to the one-photon resonance than to the three-photon resonance in THG. As is shown in Fig. 5, most of the three-photon resonance oscillator strength comes from the s -dependent part of the intraband transitions μ_s' . In Fig. 6, we show that our PPP calculation is in very good agreement with the recent calculation for octatetraene made by Soos and co-workers. Both calculations show similar two-photon and three-photon resonances. For comparison, we also display our results for the Hückel model.

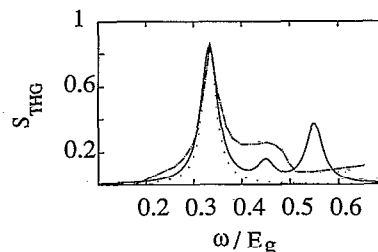


FIG. 6. A comparison of the Hückel and PPP model calculations [Eq. (57)] with Soos' PPP model calculation for THG for octatetraene $\delta=0.07$, $N=4$, $U=11.26$ eV, and $\Gamma=0.08$ eV. (Solid line) PPP calculation; (dotted line) Hückel calculation. (Dotted-dashed line) previous PPP results [Ref. 22(b)].

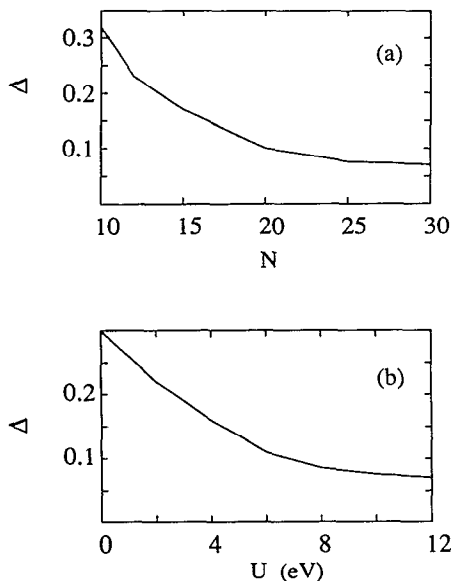


FIG. 7. The relative energy $\Delta \equiv [E(m^1A_g) - E_g]/E_g$ of the most intense m^1A_g state with respect to the band gap E_g . (a) Δ for different size N (4-30) polyacetylenes ($\delta=0.07$) with $U=11.26$ eV. (b) Δ for different interaction strength U (0-12 eV) with $N=30$.

Using the THG spectra, we have calculated the relative position $\Delta \equiv [E(m^1A_g) - E_g]/E_g$ and the oscillator strength of the most intense two-photon active state m^1A_g as a function of size N and the Coulomb interaction U . The results are displayed in Figs. 7-9. Figures 7(a) and 7(b) show that the m^1A_g state is red shifted as N or U are increased. Figures 8 and 9 show how the relative intensity of the most intense two-photon resonance compared with the single-photon band-edge transition is enhanced by the molecular size and by the Coulomb interactions, respectively.

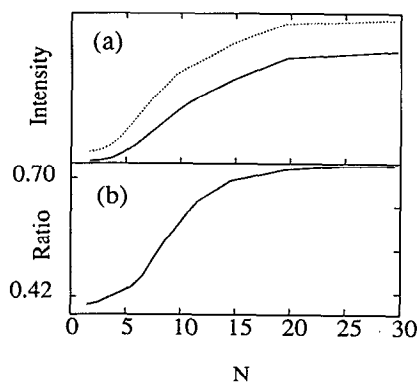


FIG. 8. The intensity of the most intense m^1A_g resonance per double bond for different N (2-30). (a) (Solid line) Intensity of the m^1A_g resonance in the PPP model for polyacetylene ($\delta=0.07$) with $U=11.26$ eV. (Dotted line) Intensity of the band gap resonance. (b) The ratio of the intensity of the m^1A_g and band gap transitions.

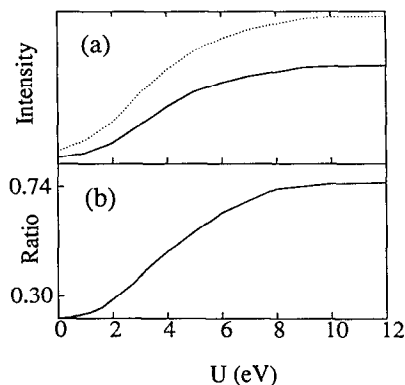


FIG. 9. The intensity of the most intense m^1A_g resonance for different values of U (0-12 eV) for polyacetylene $\delta=0.07$, $N=30$. (a) (Solid line) Intensity of the m^1A_g resonance. (Dotted line) Intensity of the band gap resonance. (b) The ratio of the intensity of m^1A_g and band gap transitions.

C. Two-photon absorption

The two-photon absorption (TPA) spectrum provides another sensitive measure of the two-photon state as pointed out by Soos and Etemad.⁴ The TPA signal (per double bond) S_{TPA} is defined as

$$S_{\text{TPA}} \equiv \text{Im}[\chi^{(3)}(\omega; \omega, -\omega, \omega)/N]. \quad (58)$$

In the top two panels of Fig. 10, we display the TPA spectra (S_{TPA}) per double bond calculated using Eq. (48) for polydiacetylene ($\delta=0.15$). The spectra show a red shift of the two-photon absorption from the ground 1^1A_g state to the 2^1A_g state, as the electron correlations are turned on. The two-photon resonance is contained in the electron Green's function $F_{s_1, s_2}(\omega_1 + \omega_2)$. This is consistent with our calculations of THG. In the bottom two panels of Fig. 10, we show $S'_{\text{TPA}} \equiv \text{Re}[\chi^{(3)}(\omega; \omega, -\omega, \omega)/N]$, which is related to the NLO refractive index. In Fig. 11(a), we show that our PPP calculation (which has no adjustable parameters) is in excellent agreement with experiment.³² The calcula-

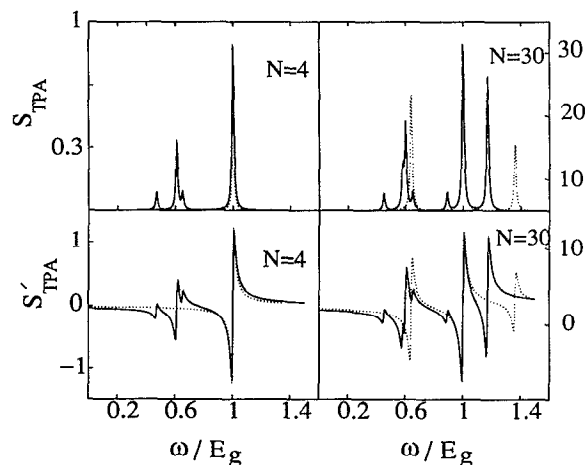


FIG. 10. Two-photon absorption per double bond for polydiacetylenes ($\delta=0.15$) with different sizes N . (Solid line) The PPP model ($U=11.26$ eV); (dotted line) the Hückel model. (Top two panels) $S_{\text{TPA}} \equiv \text{Im}[\chi^{(3)}(\omega; \omega, -\omega, \omega)/N]$ [Eq. (58)]. (Bottom two panels) $S'_{\text{TPA}} \equiv \text{Re}[\chi^{(3)}(\omega; \omega, -\omega, \omega)/N]$. $\Gamma=0.08$ eV.

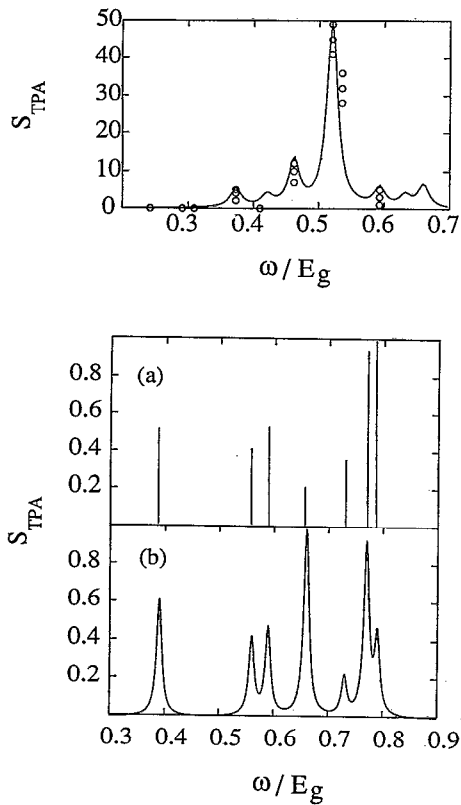


FIG. 11. (a) A comparison of the present PPP (solid curve) model calculation of TPA [Eq. (58)] for polydiacetylenes ($\delta=0.15$) with experiment (Ref. 32) (circles). $N=30$, $U=11.26$ eV, $\Gamma=0.08$ eV; (b) a comparison of the TPA calculation for polyacetylenes ($\delta=0.07$) with the calculation of Ref. 21(c). $\Gamma=0.06$ eV.

tion was made for $N=30$. The result is, however, not sensitive to that choice and corresponds to the $N \rightarrow \infty$ limit. We have verified that by repeating the calculation for $N=100$ (not shown). In Fig. 11(b), we show that our cal-

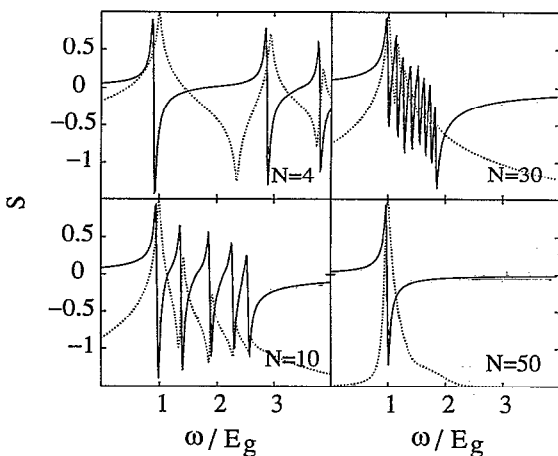


FIG. 12. (Dotted line) Linear absorption [Eq. (60)] [shown on a logarithm scale $\log(S_{\text{LA}})$] and (solid line) the electroabsorption spectra S_{EP} [Eq. (61)] for polydiacetylene ($\delta=0.15$) for different sizes using the PPP model ($U=11.26$ eV). $\Gamma=0.08$ eV.

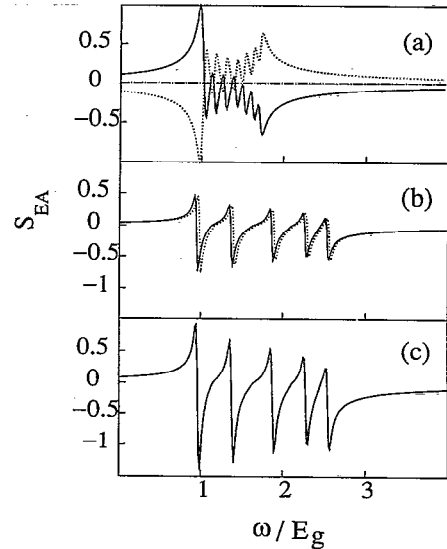


FIG. 13. Electroabsorption spectra S_{EP} [Eq. (61)] for polydiacetylene $\delta=0.15$ and $N=10$. $\Gamma=0.08$ eV. (a) The contribution from the two terms in the first summation containing the electron-hole Green's function $G_{s,s'}(\omega)$ in Eq. (63). (Solid line) the first term; (dotted line) the second term; (dashed-dotted line) the sum of the first and second terms. These terms cancel exactly. (b) The contribution from the terms containing the single electron $F_{s,s'}$ and single hole $Q_{s,s'}$ Green's function. (c) Total electroabsorption, the sum of (a) and (b).

culations of the TPA spectra also compare well with Soos' calculations.^{21(c)}

D. Electroabsorption

The difference probe absorption in the presence of an off-resonance low frequency pump (or a d.c. field) provides another useful spectroscopic technique for studying conjugated polyenes. Electroabsorption spectra have been measured for various types of materials.^{42,43} A notable feature of this absorption is the characteristic Stark shift of the resonance frequency compared to ordinary one-photon absorption. For a polydiacetylene single crystal of DCHD,

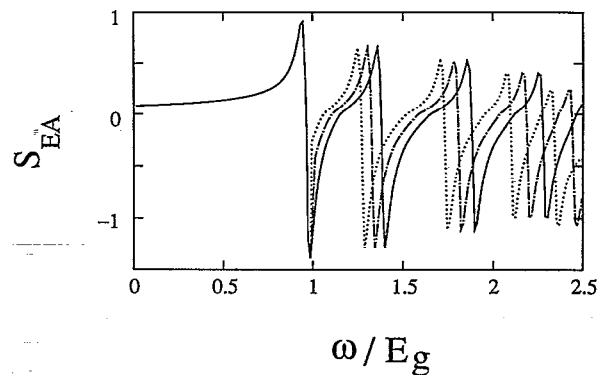


FIG. 14. Electroabsorption [Eq. (60)] for the PPP model for polydiacetylene ($\delta=0.15$, $U=11.26$ eV, and $\Gamma=0.08$ eV). (Solid line) $N=10$; (dotted-dashed line) $N=12$; (dotted line) $N=14$. The position of the resonance at $\omega/E_g=1.25$ obtained by Weiser (Ref. 42) agrees with our calculations for $N=14$.

Weiser and co-workers found red-shifted resonance below the optical band gap E_g and another electronic feature at about 1.25 of the band gap energy E_g . The electroabsorption and electroreflection properties of optical materials are important for device applications such as optical switching. The total absorption signal (per double bond) is given by

$$S_{\text{abs}} = S_{\text{LA}} + E_0^2 S_{\text{EP}}, \quad (59)$$

where the E_0 is the external off-resonant electric field. The linear absorption is

$$S_{\text{LA}} = \text{Im}[\chi^{(1)}(\omega)]/N \quad (60)$$

and the electroabsorption signal is given by

$$S_{\text{EP}} \equiv \text{Im}[\chi^{(3)}(-\omega, \omega, 0, 0)]/N \quad (61)$$

with $\chi^{(3)}(-\omega, \omega, 0, 0)$ given by

$$\chi^{(3)}(-\omega; \omega, 0, 0) = 6\rho[\gamma(\omega, 0, 0) + \gamma(-\omega, 0, 0)] \quad (62)$$

and

$$\begin{aligned} \gamma(\omega, 0, 0) = & \frac{4}{\sqrt{N}} \sum_{s's_1s_2s_3k} \sin[k(s_3 - s')/2] \mu_{s_3, s'}^c \mu_{s_3, s'}^c \mu_{s_2, k}^c \mu_{s_2, k}^c G_{s, s'}(k, \omega) [F_{s_3, s_1}(k, 0) + Q_{s_3, s_1}(k, 0)] G_{s_1, s_2}(0) E_0^2 \\ & - \frac{2}{\sqrt{N}} \sum_{s's_1s_2s_3k} \sin(ks'/2) \mu_{s_1 + s_2, s_3} \mu_{s_2, k} \mu_{s_2, k} [F_{0, s'}(k, \omega) + Q_{0, s'}(k, \omega)] F_{s', -s_1}(k, 0) G_{s_2, s_3}(0) E_0^2 \end{aligned} \quad (63)$$

Using Eqs. (61) and (63), we have calculated the electroabsorption spectrum of polydiacetylene with N ranging from 4 to 50 with $E_0 = 25$ kV/cm and polarized parallel to the molecular chain. The calculations are displayed in Fig. 12, together with the linear absorption S_{LA} which is shown for comparison. The red shift of the electroabsorption resonance compared with the linear absorption can be interpreted in term of the optical stark effect.⁴⁴ The origin of the resonance in electroabsorption may be understood as follows: the molecular eigenstates can be classified into A_g and B_u symmetry. The former are forbidden and the latter are allowed by a single-photon transition. The external electric field breaks the molecular symmetry, the states are mixed, and the selection rules are relaxed resulting in the new resonances. The modified states in the presence of the field were denoted as the *dressed states*.⁴⁴ In Fig. 13, we display the contribution of different terms to Eq. (63). The electron-hole Green's function has two contributions that interfere and exactly cancel [panel 13(a)]. The electroabsorption resonances thus originates solely from the single-electron and single-hole Green's functions $F_{s, s'}$ and $Q_{s, s'}$, which are also responsible for the two-photon resonance in the TPA and THG spectra.

In order to compare with experiment, we display in Fig. 14 the electroabsorption spectra for polydiacetylenes with various sizes. The first resonance above the band gap is at 1.25, 1.29, and 1.34 E_g for $N = 14, 12,$ and 10, respectively. The position of the band gap (E_g) and the main electroabsorption resonance at 1.25 E_g shown in Fig. 14 for $N = 14$ are in good agreement with experiment.⁴³ Our calculation suggests that the effective molecular coherence size in this experiment is $N = 14$. The experimental spectra show a few additional resonances between the band gap E_g and 1.25 E_g . These are attributed to vibrational modes, which are not incorporated in the present model, although they can be added naturally to the equations of motion by including more oscillator variables. The resonances beyond 1.5 E_g in Fig. 14 are related to transitions to higher A_g and

B_u states. No experimental data are available in this frequency region.

In conclusion, the present approach provides a unified description of nonconjugated molecules, conjugated polyenes, and semiconductor nanostructures, where the nature of the exciton changes from Frenkel to Wannier through intermediate charge-transfer excitons by simply varying the amplitude of the Coulomb interaction U and the alternation δ parameters. Our calculations demonstrate that electron correlations and interactions play a major role in the nonlinear optical response of conjugated polyenes. The origin of the two-photon resonance in the THG and TPA spectra is attributed to the combination of intraband and interband transitions. Electron correlations alter the relative energy of the one-electron transition allowed 1^1B_u state and that of the two-electron transition allowed 2^1A_g states by lowering the energy of the later. The position of the two-photon resonances obtained in THG and TPA spectra and the electroabsorption spectra provide a direct probe for this effect.

ACKNOWLEDGMENTS

The support of the Air Force Office of Scientific Research, the National Science Foundation, and the Center for Photoinduced Charge Transfer is gratefully acknowledged.

APPENDIX A: ELECTRON-HOLE REPRESENTATION OF THE PPP HAMILTONIAN

We consider the PPP Hamiltonian, i.e.,

$$H = H_0 + H', \quad (A1)$$

where H_0 is the Hückel Hamiltonian (1) and H' represents the Coulomb interactions. In the Born-Oppenheimer approximation, and when the σ electrons are incorporated

through an effective field, the Hamiltonian for $2N$ π electron H_0 can be written in terms of electron field wave operators⁴⁵ as

$$H_0 = \sum_n \int \Psi^\dagger(x) \left[-\frac{\hbar^2}{2m} \Delta_n + V_L^n(x) \right] \Psi(x) dx, \quad (\text{A2})$$

where $V_L^n(x)$ is the periodic effective potential resulting from nuclei and the σ electrons. $\Psi(x)$ is the field wave operator. The Coulomb interaction Hamiltonian can then be written as

$$H' = 1/2 \int \Psi^\dagger(x) \Psi^\dagger(x') Z(|x-x'|) \Psi(x') \Psi(x) dx' dx, \quad (\text{A3})$$

where $Z(|x-x'|)$ is the Coulomb interaction between sites x and x' .

$$Z(|x-x'|) = \frac{q^2}{(\epsilon|x-x'|)}, \quad (\text{A4})$$

where q is the electron charge and ϵ is the dielectric constant. We shall approximate the p orbitals by δ functions. We then modify the Coulomb interactions and use the Ohno formula instead

$$Z(|x-x'|) = U \{1 + [(x-x')/q^2 U]^2\}^{-1/2}. \quad (\text{A5})$$

This formula interpolates between the Coulomb expression with $\epsilon=1$ for large separation ($x-x'$) and the Hubbard interaction U at short distances. We next expand the field wave operator in the Wannier basis set (7)

$$\Psi(x) = \sum [c_n W_{c,n}(x) + d_n^\dagger W_{v,n}(x)]. \quad (\text{A6})$$

Using periodic boundary conditions for the system, $W_{v,n}(x)$ ($v=c,v$) is given by Eq. (7). Substituting expression (A6) for $\Psi(x)$ into Eqs. (A2) and (A3), we obtain Eq. (9) for H_0 and,

$$\begin{aligned} H' = 1/2 \sum_{n_1 n_2 n_3 n_4} & [c_{n_1}^\dagger c_{n_2}^\dagger c_{n_3} c_{n_4} V_{cccc}^{(n_1 n_2 n_3 n_4)} \\ & + d_{n_3} d_{n_4} d_{n_1}^\dagger d_{n_2}^\dagger V_{vvvv}^{(n_1 n_2 n_3 n_4)} - d_{n_1} c_{n_2}^\dagger c_{n_3} d_{n_4}^\dagger V_{vccv}^{(n_1 n_4 n_3 n_2)} \\ & + d_{n_1} c_{n_2}^\dagger d_{n_3}^\dagger d_{n_4} V_{cvcv}^{(n_1 n_4 n_3 n_2)} + c_{n_1}^\dagger d_{n_2}^\dagger d_{n_3}^\dagger d_{n_4} V_{cvvc}^{(n_1 n_2 n_3 n_4)}], \end{aligned} \quad (\text{A7})$$

where $V_{cvcv}^{(v_1 v_4 v_3 v_2)}$ (v_i is the band index) is given in Sec. II. Equation (14) is finally obtained by a rearrangement of Eq. (A7).

In the dipole approximation, the interaction Hamiltonian H' between the molecule and the external field can be written as

$$H_{\text{int}} = q \int P(x) \cdot E(x,t) dx, \quad (\text{A8})$$

where the polarization operator is given by

$$P(x) \equiv q \int \Psi^\dagger(x) \Psi(x) x dx. \quad (\text{A9})$$

Substituting Eq. (A6) into Eq. (A8), we obtain

$$\begin{aligned} H_{\text{int}} = -q \sum_{nm} & \left[c_n^\dagger c_m \int_0^L W_{c,n}^*(x) W_{c,m}(x) x E(x,t) dx \right. \\ & + d_n c_m \int_0^L W_{v,n}^*(x) W_{c,m}(x) x E(x,t) dx \\ & + c_n^\dagger d_m^\dagger \int_0^L W_{c,n}^*(x) W_{v,m}(x) x E(x,t) dx \\ & \left. + d_n d_m^\dagger \int_0^L W_{v,n}^*(x) W_{v,m}(x) x E(x,t) dx \right]. \end{aligned} \quad (\text{A10})$$

Where $L = Nd_0$ is the length of the polyene. When the optical wavelength is long compared with the relevant distance $n-m$, we may replace the $E(x,t)$ in the integration of Eq. (A10) by the average $E[(n+m)/2, t]$. We then obtain Eqs. (18)–(21).

APPENDIX B: COMMUTATION RELATIONS OF THE BINARY TWO-PARTICLE VARIABLES

The Fermi operators obey the basic commutation relations (8b). Applying Eq. (8b) and the definition for the two-site variables [Eq. (22)], we obtain the following commutation relations:^{26,27}

$$[C_{n_1 n_2}, Y_{nm}] \equiv C_{n_1 n_2} Y_{nm} - Y_{nm} C_{n_1 n_2} = -\delta_{n_1 m} Y_{n n_2}, \quad (\text{B1})$$

$$[C_{n_1 n_2}, Y_{nm}^\dagger] = \delta_{n_2 m} Y_{n n_1}^\dagger, \quad (\text{B2})$$

$$[D_{n_1 n_2}, Y_{nm}] = -\delta_{n_1 n} Y_{n_2 m}, \quad (\text{B3})$$

$$[D_{n_1 n_2}, Y_{nm}^\dagger] = \delta_{n_2 n} Y_{n_1 m}, \quad (\text{B4})$$

$$[Y_{n_1 n_2}, Y_{nm}^\dagger] = \delta_{n_2 m} \delta_{n_1 n} - \delta_{n_2 m} D_{n n_1} - \delta_{n_1 n} C_{m n_2}, \quad (\text{B5})$$

$$[C_{n_1 n_2}, C_{nm}] = \delta_{n_2 n} C_{n_1 m} - \delta_{n_1 m} C_{n n_2}, \quad (\text{B6})$$

$$[D_{n_1 n_2}, D_{nm}] = \delta_{n_2 n} D_{n_1 m} - \delta_{n_1 m} D_{n n_2}. \quad (\text{B7})$$

Using the transformation (D7a) to (D7c), we find that the Fermi operators obey similar commutation relations, i.e.,

$$[c_{\alpha\alpha'}, c_{\alpha'}^\dagger] = \delta_{\alpha\alpha'} - 2c_{\alpha'}^\dagger c_{\alpha}, \quad (\text{B8})$$

$$[d_{\beta\beta'}, d_{\beta'}^\dagger] = \delta_{\beta\beta'} - 2d_{\beta'}^\dagger d_{\beta}, \quad \text{others} = 0. \quad (\text{B9})$$

Equations (B1), (B7), and (8b) were used in the derivation of Eq. (24c).

APPENDIX C: EQUATIONS OF MOTION USING THE TRANSLATIONAL AND THE RELATIVE EXCITON COORDINATES

Using Eq. (13) and the Heisenberg equation of motion, we get

$$\begin{aligned}
 -i\hbar\dot{Y}_{s,k} = & -\sum_{s'} \{ \omega_{s'-s}^c \exp[-ik(s'-s)/2] - \omega_{s'-s}^v \exp[ik(s'-s)/2] + V_2(s)\delta_{s'+s} - V_1(s)\delta_{s'-s} \} Y_{s',k} + E(t)\mu_s \delta_k \\
 & -E(t) \sum_{s'} \{ \mu_{s'-s} \exp[ik(s'-s)/2] C_{s',k} + \mu_{s'+s} \exp[ik(s'+s)/2] D_{s',k} \} - 2E(t) \sum_{k'} [\mu_{s'-s}^v \delta_{k',k} + g_{k-k'} \delta_{s',s}] \\
 & \times \sin[(ks' - k's)/2] Y_{s',k'} - \frac{1}{\sqrt{N}} \sum_{s',k'} \{ 2V_1(s') \sin[(k-k')(s'-s)/2] (C_{0,k-k'} - D_{0,k-k'}) Y_{s,k'} + V_2(s-s') \\
 & \times \exp[i(k-k')s/2] C_{s'-s,k-k'} Y_{-s'+s,k'} + V_2(s-s') \exp[-i(k-k')s/2] D_{-s'+s,k-k'} Y_{s'-s,k'} \} \quad (C1a)
 \end{aligned}$$

$$\begin{aligned}
 -i\hbar\dot{C}_{s,k} = & \sum_{s'} \left\{ 2\omega_{s'-s}^c \sin[k(s'-s)/2] - [V_1(s) - V_1(0)]\delta_{s'-s} + \sum_{s''} [V_1(s'')\delta_{s,0} - V_1(s'')\delta_{s',s}] \right\} C_{s',k} \\
 & + E(t) \sum_{s'} \{ \mu_{s+s'} \exp[ik(s+s')/2] Y_{s',k}^\dagger - \mu_{s-s'} \exp[ik(-s+s')/2] Y_{s',k} \} - E(t) \sum_{s',k'} 2 \sin[(ks' - k's)/2] \\
 & \times (\mu_{s'-s}^v \delta_{k,k'} + g_{k-k'} \delta_{s,s'}) C_{s',k} \quad (C1b)
 \end{aligned}$$

$$\begin{aligned}
 -i\hbar\dot{D}_{s,k} = & \sum_{s'} \left\{ 2\omega_{s'-s}^v \sin[k(s'-s)/2] - [V_1(s) - V_1(0)]\delta_{s'-s} + \sum_{s''} [V_1(s'')\delta_{s,0} - V_1(s'')\delta_{s',s}] \right\} D_{s',k} \\
 & + E(t) \sum_{s'} \{ \mu_{s-s'} \exp[ik(s-s')/2] Y_{s',k}^\dagger - \mu_{s+s'} \exp[-ik(s+s')/2] Y_{s',k} \} + E(t) \sum_{s',k'} 2 \sin[(ks' - k's)/2] \\
 & \times (\mu_{s'-s}^v \delta_{k,k'} + g_{k-k'} \delta_{s,s'}) D_{s',k} \quad (C1c)
 \end{aligned}$$

The equation for $Y_{s,k}^\dagger$ is simply the Hermitian conjugate of Eq. (C1a). These equations are not closed once expectation values are taken. Adopting the factorization [Eq. (26)], we have

$$\langle C_{-s,k} Y_{s,k} \rangle = \langle C_{-s,k} \rangle \langle Y_{s,k} \rangle, \quad (C2)$$

$$\langle D_{-s,k} Y_{s,k} \rangle = \langle D_{-s,k} \rangle \langle Y_{s,k} \rangle. \quad (C3)$$

These factorizations close the hierarchy. Equations (C1)–(C3) were used in the calculations of the optical susceptibilities in Sec. IV.

APPENDIX D: SINGLE-PARTICLE REPRESENTATION OF $\chi^{(3)}$ FOR THE HÜCKEL MODEL

Equation (50) provides an exact expression for $\chi^{(3)}$ for the Hückel model. It is possible to recast this result using the single-particle eigenstates of the model. This alternative representation provides additional insight and will be presented below. We start by calculating the single-particle eigenstates of the Hückel Hamiltonian. The lower and higher N states will be denoted ϕ_α and ϕ_β , respectively, with energies ϵ_α and ϵ_β ($\alpha, \beta = 1, 2, \dots, N$). ϵ_α thus constitute the conduction band and are positive, whereas ϵ_β constitute the valence band and are negative. In terms of the atomic wave functions $f^{(n)}(x)$ localized at the n th carbon atom, ϕ_α and ϕ_β can be written as

$$\phi_\nu(x) = \sum_{n=1}^{2N} \hat{c}_n(\nu) f^{(n)}(x), \quad \nu = \alpha, \beta, \quad (D1)$$

where $\hat{c}_n(\nu)$ are the expansion coefficients. If we use cyclic boundary conditions, these states are equal to $\Phi_{\nu,k}$ of Sec. II. However, the following derivation does not depend on any particular choice of a boundary condition and this is why we adopt a different notation. We next introduce creation (annihilation) operators for electrons c_α^\dagger (c_α) and for holes d_α^\dagger (d_α), which create (annihilate) an electron or a hole in the α state ϕ_α , or β state ϕ_β ,

$$c_\alpha = \sum_{n=1}^{2N} \hat{c}_n(\alpha) c_n, \quad (D2)$$

$$d_\beta = \sum_{n=1}^{2N} \hat{c}_n(\beta) d_n. \quad (D3)$$

These operators satisfy the Fermi anticommutation relations which are equivalent to Eqs. (8),

$$[c_\alpha c_\alpha^\dagger]_+ = \delta_{\alpha\alpha'}, \quad [d_\beta d_\beta^\dagger]_+ = \delta_{\beta\beta'}, \quad (D4a)$$

$$[c_\alpha c_\alpha']_+ = [d_\beta d_\beta']_+ = [c_\alpha d_\beta]_+ = [c_\alpha d_\beta^\dagger]_+ = 0. \quad (D4b)$$

The Hückel Hamiltonian then reads

$$H_0 = \sum_\alpha \epsilon_\alpha c_\alpha^\dagger c_\alpha + \sum_\beta \epsilon_\beta d_\beta^\dagger d_\beta - P \cdot E(t), \quad (D5)$$

where

$$P \equiv \sum_{\alpha, \beta=1}^N (\mu_{\alpha\beta} Y_{\alpha\beta}^\dagger + \mu_{\beta\alpha} Y_{\beta\alpha}) + \sum_{\alpha, \alpha'=1}^N \mu_{\alpha\alpha'} C_{\alpha\alpha'} + \sum_{\beta, \beta'=1}^N \mu_{\beta\beta'} D_{\beta\beta'} \quad (D6)$$

and $Y_{\beta\alpha}^\dagger(t) \equiv c_\alpha^\dagger d_\beta^\dagger$, $Y_{\beta\alpha}(t) \equiv d_\beta c_\alpha$, $C_{\alpha\alpha'}(t) \equiv c_\alpha^\dagger c_{\alpha'}$, and $D_{\beta\beta'}(t) \equiv d_\beta^\dagger d_{\beta'}$. These variables are related to the binary variables in the site representation Y_{nm} , C_{nm} , and D_{nm} by the transformation

$$Y_{\beta\alpha} = \sum_{n,m}^{2N} \hat{c}_n(\alpha) \hat{c}_m(\beta) Y_{nm}, \quad (D7a)$$

$$C_{\alpha\alpha'} = \sum_{n,m=1}^{2N} \hat{c}_n(\alpha) \hat{c}_m(\alpha') C_{nm}, \quad (D7b)$$

$$D_{\beta\beta'} = \sum_{n,m=1}^{2N} \hat{c}_n(\beta) \hat{c}_m(\beta') D_{nm}. \quad (D7c)$$

$\mu_{\nu\nu'}$ are the electronic dipole matrix elements between the single-particle (electron or hole) states $\nu\nu' = \alpha\beta$, $\alpha\alpha'$, and $\beta\beta'$. The transition-dipole matrix elements $\mu_{\nu\nu'}$ are given by

$$\mu_{\nu\nu'} = \sum_{n=1}^{2N} n d_0 \hat{c}_n(\nu) \hat{c}_n^*(\nu'). \quad (D8)$$

where d_0 is the unit cell length (sum of the single and double bond lengths). Using Eq. (24) and the transformation (D7), we obtain the following *exact* equations of motion for the binary variables $Y_{\alpha\beta}$, $C_{\alpha\alpha'}$, and $D_{\beta\beta'}$:

$$-i\hbar \dot{Y}_{\alpha\beta} = (\omega_{\alpha\beta} + i\Gamma_{\alpha\beta}) Y_{\beta\alpha} + E(t) \left(\mu_{\alpha\beta} - \sum_{\alpha'} \mu_{\alpha'\beta} C_{\alpha'\alpha} \right) - E(t) \left(\sum_{\beta'} \mu_{\alpha\beta'} D_{\beta'\beta} + \sum_{\alpha'} Y_{\beta\alpha'} - \sum_{\beta'} \mu_{\beta'\beta} Y_{\beta'\alpha} \right), \quad (D9a)$$

$$-i\hbar \dot{C}_{\alpha\alpha'} = (\omega_{\alpha\alpha'} + i\Gamma_{\alpha\alpha'}) C_{\alpha\alpha'} + E(t) \times \sum_{\beta} (\mu_{\alpha'\beta} Y_{\beta\alpha}^\dagger - \mu_{\beta\alpha} Y_{\beta\alpha'}) - E(t) \times \sum_{\alpha''} (\mu_{\alpha''\alpha} C_{\alpha''\alpha'} - \mu_{\alpha'\alpha''} C_{\alpha\alpha''}), \quad (D9b)$$

$$-i\hbar \dot{D}_{\beta\beta'} = (-\omega_{\beta\beta'} + i\Gamma_{\beta\beta'}) D_{\beta\beta'} + E(t) \times \sum_{\alpha} (\mu_{\alpha\beta'} Y_{\beta\alpha}^\dagger - \mu_{\beta\alpha} Y_{\beta\alpha'}) + E(t) \times \sum_{\beta''} (\mu_{\beta\beta''} D_{\beta''\beta'} - \mu_{\beta''\beta'} D_{\beta\beta''}). \quad (D9c)$$

In Eqs. (D9), we have added phenomenological decay rates $\Gamma_{\nu\nu'}$. By setting $\Gamma_{\nu\nu'} = \Gamma$ independent on ν and ν' this becomes identical to the damping introduced in Eqs. (40)–(42). Here $\omega_{\nu\nu'} \equiv \epsilon_\nu - \epsilon_{\nu'}$ and the equation of motion of $Y_{\alpha\beta}^\dagger$ is given by Hermitian conjugation of the equation for $Y_{\alpha\beta}$. The present equations of motion thus map the calculation of the NLO response of the Hückel model onto the dynamics of coupled and driven nonlocal anharmonic oscillators analogous to the oscillators of Sec. II. A semiclassical picture of these oscillators can be obtained by introducing new variables $P_{\alpha\beta} \equiv \mu_{\beta\alpha} Y_{\beta\alpha} + \mu_{\alpha\beta} Y_{\beta\alpha}^\dagger$, $P_{\alpha\alpha'} \equiv \mu_{\alpha\alpha'} C_{\alpha\alpha'} + \mu_{\alpha'\alpha} C_{\alpha'\alpha}$, $P_{\beta\beta'} \equiv \mu_{\beta\beta'} D_{\beta\beta'} + \mu_{\beta'\beta} D_{\beta'\beta}$. The optical polarization operator thus assumes the form

$$P \equiv \sum_{\alpha, \beta=1}^N P_{\alpha\beta} + \sum_{\substack{\alpha, \alpha'=1 \\ \alpha' > \alpha}}^N P_{\alpha\alpha'} + \sum_{\substack{\beta, \beta'=1 \\ \beta > \beta'}}^N P_{\beta\beta'}. \quad (D10)$$

Equations (D9) can then be recast in terms of the polarization variables $P_{\nu\nu'}$ by a simple linear transformation

$$\ddot{P}_{\nu\nu'} = -\omega_{\nu\nu'}^2 P_{\nu\nu'} + \text{anharmonic and driving terms}, \quad \nu\nu' = \alpha\beta\alpha\alpha', \beta\beta'. \quad (D11)$$

$P_{\nu\nu'}$ thus serves as the oscillator coordinates with harmonic frequencies $\omega_{\nu\nu'}$. The anharmonic and driving terms contain cubic polynomials in $P_{\nu\nu'}$ and $E(t)$.

Proceeding along the same steps outlined in Sec. IV, these equations can be solved iteratively in the electric field, resulting in the optical susceptibilities $\chi^{(1)}$ and $\chi^{(3)}$. These are given by Eqs. (45) and (47) with

$$\alpha^0(\omega) = \sum_{\alpha, \beta} |\mu_{\alpha\beta}|^2 I_{\alpha\beta}(\omega), \quad (D12)$$

$$\begin{aligned} \gamma^0(\omega_1, \omega_2, \omega_3) = & \sum_{\alpha, \beta=1}^N \mu_{\beta\alpha} \mu_{\alpha\beta} \mu_{\beta'\alpha'} \mu_{\alpha'\beta'} \{ [I_{\alpha'\beta'}(\omega_f) - I_{\beta'\alpha'}(\omega_f)] I_{\alpha'\alpha}(\omega_1 + \omega_2) I_{\beta\alpha}(\omega_1) + [I_{\alpha'\beta'}(\omega_f) - I_{\beta\alpha'}(\omega_f)] \\ & \times I_{\beta'\beta}(\omega_1 + \omega_2) I_{\beta\alpha}(\omega_1) \} + \sum_{\alpha, \beta, \alpha', \alpha''=1}^N \mu_{\beta\alpha'} \mu_{\alpha'\alpha''} \mu_{\alpha''\alpha} \mu_{\alpha\beta} \{ [I_{\alpha\alpha''}(\omega_f) - I_{\alpha''\alpha'}(\omega_f)] I_{\alpha\alpha'}(\omega_1 + \omega_2) \\ & I_{\alpha\beta}(\omega_1) + [I_{\alpha'\beta}(\omega_f) - I_{\alpha''\alpha'}(\omega_f)] I_{\alpha''\beta}(\omega_1 + \omega_2) I_{\alpha\beta}(\omega_1) \} + \sum_{\alpha, \beta, \beta', \beta''=1}^N \mu_{\beta''\beta} \mu_{\beta'\beta''} \mu_{\beta'\alpha} \mu_{\alpha\beta} \{ [I_{\beta''\beta}(\omega_f) \\ & - I_{\beta'\beta''}(\omega_f)] I_{\beta'\beta}(\omega_1 + \omega_2) I_{\alpha\beta}(\omega_1) + [I_{\alpha\beta'}(\omega_f) - I_{\beta'\beta''}(\omega_f)] I_{\alpha\beta''}(\omega_1 + \omega_2) I_{\alpha\beta}(\omega_1) \} \end{aligned}$$

$$\begin{aligned}
& - \sum_{\alpha, \beta, \alpha', \beta'=1}^N \mu_{\beta\beta'} \mu_{\beta\alpha} \mu_{\alpha\alpha'} \mu_{\alpha'\beta'} \{ [I_{\alpha'\alpha}(\omega_f) - I_{\beta'\alpha'}(\omega_f)] I_{\beta'\alpha}(\omega_1 + \omega_2) I_{\beta\alpha}(\omega_1) + [I_{\beta\beta'}(\omega_f) \\
& - I_{\beta'\alpha'}(\omega_f)] I_{\beta\alpha'}(\omega_1 + \omega_2) I_{\beta\alpha}(\omega_1) \}, \tag{D13}
\end{aligned}$$

where

$$I_{\nu\nu'}(\omega) \equiv (\omega - \epsilon_\nu - \epsilon_{\nu'} + i\Gamma_{\nu\nu'})^{-1}, \quad \nu, \nu' = \alpha, \beta. \tag{D14}$$

If we use periodic boundary conditions, Eqs. (D12) and (D13) coincide with Eqs. (49) and (50). This equivalence is not transparent since the equations are written in a different representation. The first term in Eq. (50) corresponds to the first term in Eq. (D13). The remaining three terms of Eq. (50) correspond to the second term in Eq. (D13). Each term in Eq. (D13) corresponds to a specific excitation pathway. The interaction with the external field can be either from the left (ket) or the right (bra) side of the density matrix. When two interactions act on the same side, it is possible to produce a two-particle excitation. The two-particle excitation contribution is contained in the first term when $\alpha' = \alpha$ and $\beta' = \beta$.

The present expression for $\chi^{(3)}$ [Eqs. (49) and (D12)] together with Eq. (47) contains 32 terms each containing a fourfold summation over *single particle* electron ($a = 1, \dots, N$) or hole ($b = 1, \dots, N$) states. With permutations over the fields, the actual number is $32 \times 6 = 192$. The susceptibility $\chi^{(3)}$ is expressed in terms of multiple summa-

tions over *single-particle* (electron and hole) states. In contrast, the conventional expression for $\chi^{(3)}$ contains eight terms, each containing a fourfold summation over *molecular eigenstates* (with field permutations the number is $8 \times 6 = 48$).^{35,46} The molecular eigenstates which contribute to $\chi^{(3)}$ include the ground state, together with single-exciton and two-exciton states. The number of these states is 1, N^2 , and $N^2(N-1)^2$, respectively. In contrast, there are only $2N$ single-particle electrons and hole states. The present oscillator-based expression is thus much more compact and easy to use, particularly for large molecular sizes N where the conventional sum over molecular eigenstates expression becomes very tedious. Finally, we note that in the static limit, i.e., when all the frequencies $\omega = 0$ and in the absence of damping (setting $\Gamma_{\nu\nu'} = 0$), Eq. (D13) contains several diverging terms such as $I_{\alpha\alpha}(0)$ in which the denominator vanishes. However, when all these terms are carefully combined, the divergencies cancel exactly (as they should).⁴⁶ Equation (D13) then reduces to a simpler form

$$\begin{aligned}
\chi^{(3)}(0) = & 4\rho \sum_{\substack{\alpha, \beta, \alpha', \beta'=1 \\ \alpha' \neq \alpha}}^N [\mu_{\beta\alpha} \mu_{\alpha\beta'} \mu_{\beta'\alpha'} \mu_{\alpha'\beta} (\omega_{\alpha\beta'} + \omega_{\alpha'\beta'}) / (\omega_{\alpha'\beta'} \omega_{\alpha\beta'} \omega_{\alpha'\alpha}) \\
& - \mu_{\beta\beta'} \mu_{\beta\alpha} \mu_{\alpha\alpha'} \mu_{\alpha'\beta'} (\omega_{\alpha'\beta'} + \omega_{\alpha'\alpha}) / (\omega_{\alpha\alpha'} \omega_{\alpha'\beta'} \omega_{\alpha\beta'} \omega_{\alpha\beta})] \\
& + 4\rho \sum_{\substack{\alpha', \alpha'', \alpha, \beta=1 \\ \alpha' \neq \alpha'' \neq \alpha}}^N [\mu_{\beta\alpha''} \mu_{\alpha'\alpha''} \mu_{\alpha''\alpha} \mu_{\alpha\beta} (\omega_{\alpha\alpha''} + \omega_{\alpha'\alpha''}) / (\omega_{\alpha\alpha''} \omega_{\alpha''\alpha'} \omega_{\alpha\alpha'} \omega_{\alpha\beta}) \\
& - \mu_{\beta\alpha'} \mu_{\alpha'\alpha} \mu_{\alpha\alpha''} \mu_{\alpha''\beta} (\omega_{\alpha'\beta} + \omega_{\alpha'\alpha}) / (\omega_{\alpha\alpha'} \omega_{\alpha'\beta} \omega_{\alpha\beta} \omega_{\alpha''\beta})]. \tag{D15}
\end{aligned}$$

Equation (D15) was used in Figs. 1 and 3.

¹ *Nonlinear Optical Properties of Polyatomic Materials*, edited by D. J. Williams, (American Chemical Society, Washington, D. C., 1985, ACS Series 233.

² *Electron Properties of Polymers and Related Compounds*, edited by H. Kuzang, M. Mehing, and S. Roth (Springer, Berlin, 1985).

³ *Nonlinear Optical Properties of Organic Molecules and Crystals*, edited by D. S. Chemla and J. Zyss (Academic, Orlando, 1987), Vols. 1 and 2.

⁴ Z. G. Soos and G. W. Hayden, in *Electroresponsive and Polymeric Systems*, edited by T. A. Skothein (Marcel Dekker, New York, 1988), Vol. 1; S. Etemad and Z. G. Soos, in *Spectroscopy of Advanced Materials*, edited by R. J. H. Clark and R. E. Hester (Wiley, New York, 1991).

⁵ G. P. Agrawal, C. Cojan, and C. Flytzanis, *Phys. Rev. B* **17**, 776 (1978); C. Flytzanis, in *Nonlinear Optical Properties of Organic Molecules, and Crystals*, edited by D. S. Chemla and J. Zyss (Academic, Orlando, 1987), Vol. 2, p. 121.

⁶ Chang-qin Wu and Xin Sun, *Phys. Rev. B* **42**, 9736 (1990); Weikang Wu, *Phys. Rev. Lett.* **61**, 1119 (1988); W. K. Wu and S. Kivelson, *Synth. Met. D* **28**, 575 (1989).

⁷ (a) S. N. Dixit, D. D. Guo, and S. Mazumdar, *Mol. Cryst. Liq. Cryst.* **194**, 33 (1991); (b) S. Mazumdar and S. N. Dixit, *Synth. Met. D* **28**, 463 (1989); (c) S. Mazumdar and D. K. Campbell, *Phys. Rev. Lett.* **55**, 2067 (1985).

⁸ M. Nakano, M. Okumura, K. Yamaguchi, and T. Faeno, *Mol. Cryst. Liq. Cryst.* **182**, 1 (1990).

⁹ A. F. Garito and J. R. Heflin, F. Y. Wong, and Q. Zamani-Khamiri, in *Organic Materials for Nonlinear Optics*, edited by R. A. Hann and D. Bloor (Royal Society of Chemistry, London, 1988), Special Publication No. 69; J. R. Heflin, K. Y. Wong, O. Zamani-khamiri, and A. F. Garito, *Phys. Rev. B* **38**, 1573 (1988); *Mol. Cryst. Liq. Cryst.* **160**, 37 (1988).

¹⁰ C. P. deMelo and R. Silbey, *Chem. Phys. Lett.* **140**, 537 (1987); *J. Chem. Phys.* **88**, 2567 (1988); R. R. Chance, M. L. Shand, C. Hogy, and R. Silbey, *Phys. Rev. B* **22**, 3540 (1980).

¹¹ J. E. Gready, G. B. Bacskay, and N. S. Hush, *Chem. Phys.* **22**, 141 (1977).

- ¹²J. A. Pople, R. Krishnan, H. B. Schlegel, and J. S. Binkley, *Int. J. Quantum Chem. Symp.* **13**, 225 (1979).
- ¹³P. Jørgensen and J. Simons, *Geometric Derivatives of Energy Surface and Molecular Properties* (Reidel, Dordrecht, 1986).
- ¹⁴P. Jørgensen and J. Simons, *Second Quantization Based Methods in Quantum Chemistry* (Academic, New York, 1981).
- ¹⁵R. J. Bartlett, *J. Phys. Chem.* **93**, 169 (1989); (b) R. J. Bartlett and G. D. Purvis III, *Phys. Rev. A* **20**, 1313 (1979); F. Coester and H. Kümmel, *Nucl. Phys.* **17**, 477 (1960); G. J. B. Hurst, M. Dupuis, and E. Clementi, *J. Chem. Phys.* **89**, 385 (1988); S. P. Harna and M. Dupuis, *J. Comp. Chem.* **12**, 487 (1991).
- ¹⁶J. Zyss, *J. Chem. Phys.* **70**, 3333 (1979).
- ¹⁷L. Salem, *The Molecular Orbital of Conjugated Systems* (Benjamin, New York, 1966).
- ¹⁸J. Yu, B. Friedman, P. R. Baldwin, and W. P. Su, *Phys. Rev. B* **39**, 12814 (1989); W. P. Su, J. R. Schrieffer, and A. J. Heeger, *ibid.* **22**, 2099 (1980); S. Abe and W. P. Su, *Mol. Cryst. Liq. Cryst.* **194**, 357 (1991).
- ¹⁹I. Ohmine and M. Karplus, *J. Chem. Phys.* **68**, 2298 (1978); K. Schulten, I. Ohmine, and M. Karplus, *ibid.* **64**, 4422 (1976).
- ²⁰(a) B. S. Hudson and B. E. Kohler, *Chem. Phys. Lett.* **14**, 299 (1972); (b) *J. Chem. Phys.* **59**, 4984 (1973); (c) B. S. Hudson, B. E. Kohler, and K. Schulten, *Excited States* **6**, 1 (1982); B. E. Kohler, *J. Chem. Phys.* **93**, 5838 (1990).
- ²¹(a) Z. G. Soos and S. Ramasheba, *J. Chem. Phys.* **90**, 1067 (1988); (b) *Phys. Rev. B* **29**, 5410 (1984); (c) P. C. M. McWilliams, G. W. Hayden, and Z. G. Soos, *ibid.* **43**, 9777 (1991).
- ²²(a) W.-S. Fann, S. Benson, J. M. Madey, S. Etemad, G. L. Baker, and F. Kajzar, *Phys. Rev. Lett.* **62**, 1492 (1989); (b) P. D. Townsend, W.-S. Fann, S. Etemad, G. L. Baker, Z. G. Soos, and P. C. M. McWilliams, *Chem. Phys. Lett.* **180**, 485 (1991).
- ²³(a) F. C. Spano and S. Mukamel, *Phys. Rev. Lett.* **66**, 1197 (1991); (b) O. Dubovsky and S. Mukamel, *J. Chem. Phys.* **95**, 7828 (1991); (c) J. Knoester and S. Mukamel, *Phys. Rep.* **205**, 1 (1991).
- ²⁴F. C. Spano and S. Mukamel, *Phys. Rev. A* **40**, 5783 (1989); O. Dubovsky and S. Mukamel, *J. Chem. Phys.* **96**, 9201 (1992).
- ²⁵S. Schmitt-Rink, D. A. B. Miller, and D. S. Chemla, *Phys. Rev. B* **35**, 8113 (1987); F. F. So, S. R. Forrest, Y. Q. Shi, and W. H. Steier, *Appl. Phys. Lett.* **56**, 674 (1990); D. Mobius and H. Kuhn, *Isr. J. Chem.* **18**, 375 (1979); *J. Appl. Phys.* **64**, 5138 (1988); *Langmuir-Blodgett Films*, edited by G. Roberts (Plenum, New York, 1990); M. G. Bawendi, M. L. Steigerwald, and L. E. Brus, *Annu. Rev. Phys. Chem.* **41**, 477 (1990); Y. Wang, *J. Opt. Soc. Am. B* **8**, 981 (1991).
- ²⁶A. Stahl and D. Baslev, *Electrodynamics of the Semiconductor Band Edge* (Springer, Berlin, 1987).
- ²⁷J. R. Kuklinsky and S. Mukamel, *Phys. Rev. B* **42**, 295 (1990).
- ²⁸H. X. Wang and S. Mukamel, *Chem. Phys. Lett.* **192**, 417 (1992).
- ²⁹J. P. Hermann and J. Ducuing, *J. Appl. Phys.* **45**, 5100 (1974).
- ³⁰T. Kurihara, N. Oba, Y. Mori, S. Tomaru, and T. Kaino, *J. Appl. Phys.* **70**, 1 (1991).
- ³¹S. A. Jenekhe, M. F. Roberts, A. K. Agrawal, J. S. Meth, and H. Vanherzeele, *Mater. Res. Soc. Symp. Proc.* **214**, 55 (1991).
- ³²W. E. Torruellas, D. Neher, R. Zanoni, G. I. Stegeman, and F. Kajzar, *Chem. Phys. Lett.* **175**, 11 (1990); W. E. Torruellas, K. B. Rochford, R. Zanoni, S. Aramaki, and G. I. Stegeman, *Opt. Commun.* **82**, 94 (1991); S. Aramaki, W. Torruellas, R. Zanoni, and G. I. Stegeman, *ibid.* **85**, 527 (1991).
- ³³(a) G. J. Blanchard, J. P. Heritage, A. C. Von Lehmen, M. K. Kelly, G. L. Baker, and S. Etemad, *Phys. Rev. Lett.* **63**, 887 (1989); (b) B. I. Greene, J. F. Mueller, J. Orenstein, D. H. Rapkine, S. Schmitt-Rink, and M. Thakur, *Phys. Rev. Lett.* **61**, 325 (1988); B. C. Hess, G. S. Kanner, Z. V. Vardeny, and G. L. Baker, *Phys. Rev. Lett.* **66**, 2364 (1991).
- ³⁴T. Hasegawa, Y. Iwasa, H. Kishida, T. Koda, Y. Tokura, H. Tachibana, and Y. Kawabata, *Phys. Rev. B* **45**, 6317 (1992); J. R. G. Thorne, Y. Ohsako, J. M. Zeigler, and R. M. Hochstrasser, *Chem. Phys. Lett.* **162**, 455 (1989); Z. G. Soos and R. G. Kepler, *Phys. Rev. B* **43**, 11908 (1991); Y. Moritomo, Y. Tokura, H. Tachibana, Y. Kawabata, and R. D. Miller, *ibid.* **43**, 14746 (1991).
- ³⁵N. Bloembergen, *Nonlinear Optics* (Benjamin, New York, 1965).
- ³⁶S. Mukamel and H. X. Wang, *Phys. Rev. Lett.* **69**, 65 (1992); H. X. Wang and S. Mukamel, *Nonlinear Optics* (in press); S. Mukamel and H. X. Wang, in *Optics of Semiconductor Nanostructures*, edited by F. Henneberger and S. Schmitt-Rink (in press).
- ³⁷B. I. Greene, J. Orenstein, and S. Schmitt-Rink, *Science* **247**, 679 (1990).
- ³⁸P. Ring and P. Schuck, *The Nuclear Many-Body Problem* (Springer, Berlin, 1980).
- ³⁹S. Mukamel, *Adv. Chem. Phys.* **70**, 165 (1988).
- ⁴⁰(a) Z. Shuai and J. L. Brédas, *Phys. Rev. B* **44**, 5962 (1991); (b) D. N. Beratan, J. N. Onuchic, and J. W. Perry, *J. Phys. Chem.* **91**, 2696 (1987).
- ⁴¹E. N. Economou, *Green's Functions in Quantum Physics* (Springer, Berlin, 1983).
- ⁴²L. Sebastian and G. Weiser, *Chem. Phys. Lett.* **62**, 447 (1981).
- ⁴³K. Ishikawa, T. Koda, Y. Tokura, and T. Kotaka, *Synth. Met.* **41**, 221 (1991); R. G. Kepler and Z. G. Soos, *ibid.* **41**, 1563 (1991); O. M. Gelsen, D. D. C. Bradley, H. Murata, T. Tsutsui, S. Saito, J. Ruhe, and G. Wegner, *ibid.* **41**, 875 (1991); Y. Kawabe, F. Jarka, N. Peygabarjan, D. Guo, S. Mazumdar, S. N. Dixit, and F. Kajzar, *Phys. Rev. B* **44**, 6530 (1991).
- ⁴⁴A. Mysyrowicz, D. Hulin, A. Antonetti, A. Migus, W. T. Masselink, and H. Morkoc, *Phys. Rev. Lett.* **56**, 2749 (1986).
- ⁴⁵H. Haken, *Quantum Field Theory of Solids* (North-Holland, Amsterdam, 1983).
- ⁴⁶B. J. Orr and J. F. Ward, *Mol. Phys.* **20**, 513 (1971).